



**HAL**  
open science

# Influence of phyllosilicates on the hydrothermal alteration of organic matter in asteroids: Experimental perspectives

V. Vinogradoff, C. Le Guillou, S. Bernard, J.C. C Viennet, M. Jaber, L. Remusat

## ► To cite this version:

V. Vinogradoff, C. Le Guillou, S. Bernard, J.C. C Viennet, M. Jaber, et al.. Influence of phyllosilicates on the hydrothermal alteration of organic matter in asteroids: Experimental perspectives. *Geochimica et Cosmochimica Acta*, 2019, 10.1016/j.gca.2019.10.029 . hal-02341302

**HAL Id: hal-02341302**

**<https://hal.science/hal-02341302v1>**

Submitted on 12 Nov 2019

**HAL** is a multi-disciplinary open access archive for the deposit and dissemination of scientific research documents, whether they are published or not. The documents may come from teaching and research institutions in France or abroad, or from public or private research centers.

L'archive ouverte pluridisciplinaire **HAL**, est destinée au dépôt et à la diffusion de documents scientifiques de niveau recherche, publiés ou non, émanant des établissements d'enseignement et de recherche français ou étrangers, des laboratoires publics ou privés.

## Journal Pre-proofs

Influence of phyllosilicates on the hydrothermal alteration of organic matter in asteroids: experimental perspectives

V. Vinogradoff, C. Le Guillou, S. Bernard, J.C. Viennet, M. Jaber, L. Remusat

PII: S0016-7037(19)30683-0  
DOI: <https://doi.org/10.1016/j.gca.2019.10.029>  
Reference: GCA 11497

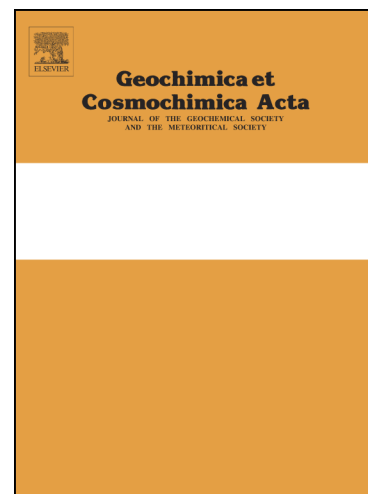
To appear in: *Geochimica et Cosmochimica Acta*

Received Date: 4 June 2019  
Revised Date: 19 October 2019  
Accepted Date: 19 October 2019

Please cite this article as: Vinogradoff, V., Le Guillou, C., Bernard, S., Viennet, J.C., Jaber, M., Remusat, L., Influence of phyllosilicates on the hydrothermal alteration of organic matter in asteroids: experimental perspectives, *Geochimica et Cosmochimica Acta* (2019), doi: <https://doi.org/10.1016/j.gca.2019.10.029>

This is a PDF file of an article that has undergone enhancements after acceptance, such as the addition of a cover page and metadata, and formatting for readability, but it is not yet the definitive version of record. This version will undergo additional copyediting, typesetting and review before it is published in its final form, but we are providing this version to give early visibility of the article. Please note that, during the production process, errors may be discovered which could affect the content, and all legal disclaimers that apply to the journal pertain.

© 2019 Elsevier Ltd. All rights reserved.



## Influence of phyllosilicates on the hydrothermal alteration of organic matter in asteroids: experimental perspectives.

V. Vinogradoff<sup>1,2\*</sup>, C. Le Guillou<sup>3</sup>, S. Bernard<sup>2</sup>, J.C. Viennet<sup>2</sup>, M. Jaber<sup>4</sup> and L. Remusat<sup>2</sup>

<sup>1</sup> Aix-Marseille Université, UMR CNRS 7345, Physique des interactions ioniques et moléculaires, PIIM. \* [vassilissa.vinogradoff@univ-amu.fr](mailto:vassilissa.vinogradoff@univ-amu.fr)

<sup>2</sup> Muséum National d'Histoire Naturelle, UMR CNRS 7590, Sorbonne Université, Institut de Minéralogie, Physique des Matériaux et Cosmochimie, IMPMC, Paris, France.

<sup>3</sup> Univ. Lille, CNRS, INRA, ENSCL, UMR 8207 - UMET - Unité Matériaux et Transformations, F-59000 Lille, France.

<sup>4</sup> Sorbonne Université, Laboratoire d'Archéologie Moléculaire et Structurale, LAMS, UMR CNRS 8220, Paris, France.

### Abstract

**The origin of the diverse organic compounds present in carbonaceous chondrites (CC) remains uncertain. We aim at investigating the role that hydrothermal alteration may have had on the molecular evolution of organic matter (OM). In particular, within CC matrices, OM is intimately embedded within phyllosilicates down to the nanometer scale, which raises the question of the influence of phyllosilicates on OM transformation during hydrothermal alteration on parent bodies. We conducted hydrothermal experiments at 150°C and alkaline pH, using a well-known molecule present in processed interstellar ice analogues, the hexamethylenetetramine (HMT), in the presence of Al- and Fe-rich smectites. Experimental products were characterized by gas chromatography mass spectrometry, infrared spectroscopy, X-ray diffraction and synchrotron-based X-ray absorption near edge structure spectroscopy. Within 31 days, the HMT+smectites+H<sub>2</sub>O system leads to (1) the formation of a diverse suite of soluble organic compounds, yet less abundant and less complex than in the absence of smectite, (2) carbon-rich smectite residues (3.8 wt.% and 2.6 wt.% of carbon for the Al- and Fe-rich smectite residues, respectively). In addition, the abundance and molecular composition of the final organic compounds depend on the nature of the phyllosilicate (Al vs. Fe-smectite). Various and complex interaction mechanisms could occur between OM and smectite. Physisorption, chemisorption and intercalation**

**processes have likely entrapped a significant portion of the organic compounds, thereby altering their chemical evolution. The present work demonstrates that the presence and the nature of phyllosilicates influences the reaction pathways of organic compounds during hydrothermal alteration and that the presence of organic compounds may impact the mineral assemblage. This could have had significant importance for the co-evolution of OM and mineral phases in primitive bodies during hydrothermal alteration.**

## 1 Introduction

The origin of the wide range of organic compounds found in carbonaceous chondrites (CC) is a major question in cosmochemistry that is complex to disentangle. Whereas some molecules in CC could be inherited from the interstellar medium (ISM), synthesis and chemical evolutions in the solar nebula and in the asteroidal parent body can also have contributed to the present molecular distribution (Remusat, 2016; Alexander et al., 2017). Asteroidal parent bodies of CC have accreted organic matter (OM) and some CCs contain up to 3-5 wt. % of organic carbon (Robert and Epstein, 1982; Pearson et al., 2006; Alexander et al., 2007). Acid treatment on one hand and solvent extraction on the other revealed in CC the presence of both insoluble organic matter (IOM) and soluble organic matter (SOM) in ratios ranging from 90/10 to 70/30 wt.% (Sephton, 2014; Remusat, 2016; Alexander et al., 2017). The SOM is composed of small organic molecules (carboxylic acids, amino acids, nucleobases, aliphatic and polycyclic aromatic hydrocarbons, sugars) (Pizzarello et al., 2006) and the IOM is constituted of macromolecules containing heteroatoms (N, S, O) (Sephton et al., 2000; 2004; Remusat et al., 2005; Derenne and Robert, 2010).

The parent asteroids of CC have experienced hydrothermal alteration after accretion (Brearley, 2006). The alteration of primary mineral phases has been documented (e.g., formation of phyllosilicates, carbonates, sulfates...), but the amplitude of OM processing remains an open field of investigations (Alexander et al., 2007; Cody et al., 2011; Orthous-Daunay et al., 2013; Le Guillou and Brearley, 2014; Vollmer et al., 2014; Remusat, 2016; Elsila et al., 2016; Aponte et al., 2016; Changela et al., 2018; Vinogradoff et al., 2018). Studies have pointed that bulk IOM transformation occurred inside parent bodies, and that SOM content and chemistry also evolves with increasing hydrothermal alteration (quantity of water, duration, temperature...), as for instance for the Tagish Lake chondrite (Herd et

al., 2011; Glavin et al., 2012; Hiltz et al., 2014; Alexander et al., 2014). *In-situ* observations of this OM have revealed at least two different population of OM: sub-micrometric OM particles and diffuse OM finely interspersed within phyllosilicates (Busemann et al., 2006; Garvie and Buseck, 2007; De Gregorio et al., 2013; Le Guillou et al., 2014; Le Guillou and Brearley, 2014; Vollmer et al., 2014; Vinogradoff et al., 2017; Changela et al., 2018). Some of the chemical and morphological signatures of this OM could hence be related to asteroidal alteration, including hydrothermal reactions with minerals.

In order to better constrain the impact of hydrothermal alteration on complex organic systems, recent experimental studies have focused on the evolution of simple molecules, such as formaldehyde with glycolaldehyde and ammonia (Kebukawa et al., 2013; Kebukawa et al., 2017) and hexamethylenetetramine (Vinogradoff et al., 2018). These studies suggested that complex chemical reactions occur during hydrothermal processing, leading to the formation of a large diversity of soluble compounds, as well as to the production of some insoluble material. However, in chondrites, OM is intimately associated with amorphous mineral phases and phyllosilicates (Garvie and Buseck, 2007; Le Guillou et al., 2014; Le Guillou and Brearley, 2014; Vollmer et al., 2014; Vinogradoff et al., 2017) which could have an impact on the OM reactivity during hydrothermal alteration. Here, we experimentally investigate the influence of phyllosilicates on the hydrothermal reactivity of OM in asteroidal conditions.

Part of the OM accreted in CC might originate from the evolution of organic-rich dust ices constituent of the cold interstellar medium (ISM) (Caselli and Ceccarelli, 2012; Gudipati et al., 2015). Laboratory experiments are commonly conducted to simulate this primary transformation of the OM during ices evolution from dense molecular clouds to early solar nebula phases (Allamandola et al., 1988; Bernstein et al., 1995). After processing by UV irradiation and warming (10 K to 300 K), ices containing simple molecules such as methanol, ammonia and water lead to refractory complex organic residues at room temperature (Muñoz Caro and Schutte, 2003; Danger et al., 2013). Here, we selected the main organic product formed in these organic residues: hexamethylenetetramine (HMT- $C_6H_{12}N_4$ ) (Bernstein et al., 1995; Muñoz Caro and Schutte, 2003; Vinogradoff et al., 2011; 2013; 2015), as representative molecule of this evolution of interstellar ices. HMT is thermodynamically favored (lowest energy state) when precursors such as methanol and ammonia are used and is stable as a solid up to 130-230 °C at low pressure ( $10^{-8}$  mbar) (Vinogradoff et al., 2012). HMT has not been observed in astrophysical environment or in

meteorites yet, but multiple scenarios can account for its possible accretion in CC parent bodies (Vinogradoff et al., 2013; 2015).

We selected smectites to conduct the present experiments because they are observed in various chondrites groups such as CI, CM, CR carbonaceous chondrites and ordinary chondrites (Alexander et al., 1989; Brearley, 2006; Beck et al., 2010; Howard et al., 2011; Le Guillou et al., 2015). They have a strong interaction potential due to their 2:1 structure, high swelling properties and high cationic exchange capacity (Lagaly et al., 2013). Smectites have an impact on the chemical evolution of organic compounds (Schoonen et al., 2004; Williams et al., 2005; Ganor et al., 2009; Drouin et al., 2010; Saladino et al., 2010; Poch et al., 2015). Surface reactions and inter-layer space reactivity are the main mechanisms involved to explain the role of absorbent, protector or catalyst of smectites on the OM (Schoonen et al., 2004; Ganor et al., 2009). In this study, we compared the impact of two synthetic smectites of different composition on the HMT transformation in asteroidal conditions. We choose an aluminium-magnesium-bearing smectite, frequently used to study the organo-clay interaction (Wang and Lee, 1993; Saladino et al., 2010; Montgomery et al., 2011; Fuchida et al., 2014; Jaber et al., 2014; Watson and Sephton, 2015), as well as an iron-bearing smectite, to investigate the roles of the smectite composition and structure.

At the end of the 31 days long experiments, soluble organic compounds were characterized by gas chromatography coupled to mass spectrometry (GC-MS), while the solid residue was characterized by elemental analysis (EA), Fourier-transform infrared spectroscopy (FTIR), X-ray diffraction (XRD), and scanning transmission X-ray microscopy (STXM). Based on the comparison with experiments conducted in the absence of phyllosilicates (Vinogradoff et al., 2018), the present study demonstrates the major influence of the presence and the nature of phyllosilicates on the hydrothermal reactivity of HMT. In other words, phyllosilicates may have played a major role in the evolution of chondritic organic matter.

## 2 Methods

### 2.1 Synthesis of phyllosilicates

Diocahedral Al-rich and Fe-rich 2:1 smectite were synthesized for the present study (Fig. 1). The Al-rich 2:1 smectite was synthesized by mixing deionized water, hydrofluoric acid, sodium fluoride, Mg acetate tetrahydrate, Al and Si (Jaber et al., 2014). Sodium fluoride

was used to reach a higher crystallinity. The hydrogel was kept for 2 hours at room temperature and then introduced into a poly-(tetrafluoroethylene)-lined stainless-steel autoclave (PTFE reactor) and heated at 200 °C for 72 h. Products were recovered by filtration, washed thoroughly with distilled water, and dried at 60 °C for 12 hours. The structural formulae per half unit cell is similar to montmorillonite:  $\text{Na}_{0.3}[\text{Mg}_{0.3}\text{Al}_{1.7}]\text{Si}_4\text{O}_{10}(\text{OH}_{1.5},\text{F}_{0.5}) \cdot x\text{H}_2\text{O}$ . This phyllosilicate is called Al-rich smectite in this work.

The Fe-rich 2:1 smectite was synthesized following the protocol of Andrieux & Petit (2010) by mixing sodium metasilicate, aluminum chloride, iron chloride and magnesium chloride. The average composition measured by a multi-technical approach, including Mossbauer and X-Ray fluorescence, is  $\text{Na}_{0.42}(\text{Si}_{3.60}\text{Al}_{0.38}\text{Fe}_{0.02})(\text{Al}_{0.18}\text{Fe}_{1.80}\text{Mg}_{0.02})\text{O}_{10}(\text{OH})_2 \cdot x\text{H}_2\text{O}$ , hereafter called Fe-rich smectite.

## 2.2 Experimental and analytical procedures

### 2.2.1 Experimental setup

Solutions containing HMT and phyllosilicates were heated at 150 °C for 31 days in closed systems ( $P_{\text{sat}} = 6$  bars). Bi-distilled water, equilibrated with KOH ( $10^{-4}$  M) to reach pH 10, was degassed with Argon before experiments. Starting mixtures were prepared under argon atmosphere (> 99.999 %; Air Liquide, ALPHAGAZ 1) in a glove box (< 0.5 ppm  $\text{O}_2$ ) and loaded into sealed 23 mL PTFE reactors. HMT powder (> 99 % - Sigma Aldrich) was dissolved in 1 mL of water to obtain a concentration of 0.7 M, which is below the saturation point of HMT in water ( $853 \text{ g}\cdot\text{L}^{-1}$  at 25 °C), and mixed with 100 mg of synthetic phyllosilicate. Reactors were then put in oven with temperature accurately regulated at 150°C. At the end of the experiments, the pH values were comprised between 8 and 9 for the Al and Fe-rich smectite solutions.

Experiments without HMT were carried out for 20 days under the same experimental conditions. The HMT and the smectite were also mixed together at 25 °C, stirred regularly during 24 h and then the phyllosilicate powder was extracted the same way as the hydrothermal experiments (centrifuged, washed with solvents and dried). These mixtures stand as references and are hereafter called starting material.

### 2.2.2 Analytical protocol

After the completion of the experiments, different portions of the samples were processed separately (Fig. 2). Hydrothermal products were centrifuged in Eppendorf tubes (2 mL, 6 minutes at 12,000 rpm). The liquid phase was split into two aliquots. Liquid-liquid extraction was performed using 0.5 mL of dichloromethane (DCM) on a 0.5 mL aliquot, which concentrates mainly the non-polar soluble compounds. GC-MS analysis was performed on the DCM extract. The solid residue was successively washed and sonicated two times in a bath (3 min.) with each of the following solvents: water, methanol (CH<sub>3</sub>OH), and DCM/CH<sub>3</sub>OH (1:1 vol./vol.) for a total of six extractions (2 mL of final solvent volume). The solid residues were then dried in an oven for at least 24h at 60 °C under primary vacuum.

## 2.3 Characterization techniques

### 2.3.1 Specific surface area (BET analysis)

Measurements of the specific surface areas were conducted on both synthesized smectites. We used the nitrogen adsorption methods with a BELSORP mini-II instrument operated at the Institut de Minéralogie de Physique des Matériaux et de Cosmochimie (IMPMC) in Paris, France. About 332 mg of sample were cooled down at 77 K and subjected to a saturated vapor pressure of 97 kPa of N<sub>2</sub> during 24 hours. The Brunauer-Emmett-Teller (BET) adsorption method was used for data treatment. Specific surface area ( $S_{\text{BET}}$ ) were calculated based on the regression line of the adsorption isotherm following the BET equation:  $S_{\text{BET}} = N \cdot s / ((A+I) \cdot V \cdot a)$  where N is Avogadro's number, s the adsorption cross-section of the adsorbed species, A the slope, I the y-intercept, V the molar volume of adsorbate gas and a the mass of the solid sample.

### 2.3.2 Elemental analysis

The hydrogen, nitrogen and carbon contents of the solid residue after 31 days of hydrothermal experiments were determined using a Thermo-Fisher Flash 2000 CHNS-O analyzer at the Institut de sciences de la Terre de Paris (ISTeP) in Paris, France. 2.8 mg of the residue of the experiment conducted with the Fe-rich smectite, and 3.2 mg of the residue of the experiment conducted with the Al-rich smectite was combusted under oxygen/helium flux at 960 °C. N<sub>2</sub>, CO<sub>2</sub>, and H<sub>2</sub>O released by combustion were separated by a chromatography column and quantified using a thermal conductivity detector. Different soil

samples were used as standards. Uncertainties are 0.02 wt% for N, 0.07 wt% for C and 0.03 wt% for H using standard calibration.

### 2.3.3 GC-MS analysis

Compounds soluble in DCM were analyzed without derivatization, using an Agilent Technologies 6890N gas chromatograph coupled with an Agilent Technologies 5973 network mass spectrometer operated at the laboratory Milieux environnementaux, transferts et interactions dans les hydrosystèmes et les sols (METIS) in Paris, France. The GC was equipped with a RTX-5Si/MS (30 m x 0.25 mm, 0.5  $\mu\text{m}$  film) capillary column coated with chemically bound Restek (low-polarity phase, suitable for semi-volatile, hydrocarbon, amine, phenol compounds). The injection temperature was 280°C in splitless mode and the GC oven programmed from 50°C to 320°C, ramping at 4°C/min, and using He as gas carrier. The solvent delay was as short as possible (3 minutes). The mass spectrometer was operated at an electron energy of 70 eV, an ion source temperature of 220°C and a scanning conditions from 35 to 700 amu at 2.24 scan.s<sup>-1</sup>. Products were identified using the NIST database. Data processing was done using the OpenChrom software, namely subtraction of the solvent background (DCM) taken at 3.8 min followed by an automatic peak detection using the MSD first derivative process (signal to noise ratios, S/N > 3). This procedure allowed to quantify the number of species detected by GC-MS. Each peak of the total ion current was integrated using the MSD integrator option to quantify the abundance of each species detected by GC-MS. Compounds detected between 5 and 25 minutes have a lower  $m/z$  than HMT (< 140  $m/z$ ) and are called low molecular weight compounds (LC) in comparison to the compounds detected between 25 and 54 minutes which have higher  $m/z$  than HMT (>140  $m/z$ ), which we call the high molecular weight compounds (HC).

### 2.3.4 X-ray diffraction (XRD)

The XRD patterns were collected at the X-ray diffraction facility of IMPMC (Paris, France). The X-ray powder diffraction patterns were recorded using an X'Pert Pro Panalytical diffractometer equipped with a CoK $\alpha_{1,2}$  radiation source ( $\lambda\text{K}\alpha_1 = 1.78897 \text{ \AA}$ ,  $\lambda\text{K}\alpha_2 = 1.79285 \text{ \AA}$ ) and an X'Celerator detector, in Bragg Brentano geometry (0.04° Soller slits, 0.5° programmable divergence slit, 1° incident antiscatter slit, and 0.5° diffracted antiscatter slit). The XRD patterns were collected between 3 and 60° 2 $\theta$  with a step size of 0.0167° 2 $\theta$  and a counting time per step of 6.7 s. Less than 0.5 mg of grinded samples were

placed on a Si pellet and introduced in the diffractometer. The analysis on the pellet may have influenced the profile of diffraction pattern due to random geometry of the phyllosilicate.

### 2.3.5 Infrared spectroscopy

FTIR analyses were performed using a Vertex 70 spectrometer (Bruker) at the Musée de l'Homme (Paris, France). Around 0.5 mg of powdered sample was pressed onto a diamond crystal surface using a single reflection in the attenuate total resonance device, ATR-quest (Specac). The spectrum was acquired from 370 to 4000  $\text{cm}^{-1}$  with a spectral resolution of 4  $\text{cm}^{-1}$ . Ninety-six spectra were accumulated (vs. 128 for the background). Each IR spectrum was corrected with a linear elastic concave baseline and normalized to its total absorbance area (using Bruker Opus software).

### 2.3.6 Scanning transmission X-ray microscopy (STXM) and X-ray absorption near-edge structure (XANES) spectroscopy.

STXM-XANES analyses were performed at the HERMES beamline at the synchrotron SOLEIL (Saclay, France). The microscope chamber was evacuated to 100 mTorr after sample insertion and filled with helium. Measurements were performed using the low energy grating and a circularly polarized light. Energy calibration was accomplished using the 3p Rydberg peak at 294.96 eV of gaseous  $\text{CO}_2$ . XANES spectra were obtained by collecting image stacks, i.e. by rastering the beam over the sample. Stacks were collected with a dwell time of one millisecond per pixel to avoid irradiation damage, with a spectral resolution of 0.1 eV over the carbon XANES region (283-293 eV), of 0.2 eV over the Nitrogen XANES region (398-410 eV) and of 1 eV otherwise. Extraction of spectra were done using the aXis2000 software, before normalization to the carbon content performed thanks to the QUANTORXS program (Le Guillou et al., 2018).

## 3 Results

### 3.1 Evolution of the soluble fraction

Soluble compounds were analyzed by GC-MS on the DCM liquid-liquid extracts (Fig. 2). The GC-MS chromatograms of the control sample (smectite without HMT) do not exhibit any peak, indicating the absence of organic contamination (data not shown). The

GC-MS chromatogram of the DCM fraction of the starting material displays one peak at 20.73 min corresponding to pure HMT ( $m/z$  140; Fig. 3). After 31 days of hydrothermal treatment, the HMT peak is no longer observed, but new peaks are observed, instead. The diversity of compounds detected in the DCM extract (Fig. 3) of the Al-rich smectite+HMT sample (104 peaks) and in the Fe-rich smectite+HMT sample (56 peaks) is lower than for experiments conducted in the absence of smectites (150 peaks were detected) (Vinogradoff et al., 2018). In addition, this number is two times lower for the extract from the Fe-rich smectite sample than that of the experiments conducted with the Al-rich smectite.

The identified light compounds (LC) in both HMT+phyllosilicate chromatograms of the DCM fractions (released between 5 and 25 minutes, with  $m/z$  up to 136) are mainly nitrogen-bearing cyclic molecules with increasing methyl substituents (table 1). LC consist mainly of three families of nitrogen-bearing molecules: pyridine derivative molecules (6 membered ring molecules –  $C_5H_5N$ +alkyl substituents), imidazole/pyrazole derivative molecules (5 membered ring molecules –  $C_3H_4N_2 \pm$  alkyl substituents), and pyrazine derivative molecules (6-membered ring molecules –  $C_4H_4N_2 \pm$  alkyl substituents). Less abundant, oxygen-bearing compounds are also observed, such as the N,N-dimethyl formamide, which is one of the first product to be formed during experiments conducted in the absence of smectites (Vinogradoff et al., 2018). Species detected after 25 minutes on the chromatograms (called heavy compounds or HC) are identified as derivatives of the LC compounds (with more substituents) or as polymerized LC. Different relative peak intensities are observed (Fig. 3) in the chromatograms of the Al and Fe-rich smectite extracts, indicating different relative abundances of the LC and HC. Noteworthy, the compounds detected in the DCM fractions may not fully be representative of the whole organic soluble compounds produced in the experiments, as some polar compounds may not be detected with our GC-MS procedure.

## 3.2 Evaluation of the solid fraction

### 3.2.1 Specific surface areas

The Fe-rich smectite has a specific surface area (external and interlayer space) of 42  $m^2/g$  while the Al-rich smectite 77  $m^2/g$ , (Table 2). The initial amount of added HMT is  $4.3 \times 10^{20}$  molecules. According to Connolly (Connolly, 1983), HMT molecular surface (morphology of 4 faces) is approximately  $1.35 \times 10^{-18}$   $m^2/molecule$  and the area occupied by one molecule on the phyllosilicate surface is quarter of its total molecular surface

( $3.38 \times 10^{-19}$  m<sup>2</sup>/molecule). Hence, the total surface area potentially covered by HMT molecules in the initial mixture is thus  $\sim 145$  m<sup>2</sup>. This surface is about 18-32 times larger than the available surface of the Fe-rich smectite and Al-rich smectite (4.2 m<sup>2</sup> and 7.7 m<sup>2</sup>, respectively). This corresponds to a maximum of 3 and 6% of the initial amount of HMT molecules that could occupy the surfaces.

### 3.2.2 Elemental analysis

Elemental analyses of the 31-day solid residues (table 3) reveal that after solvent extraction, the Fe-rich and Al-rich smectite have respectively retained 2.6 wt.% and 3.9 wt.% of organic carbon. Nitrogen, which is also quite abundant, is 1.4 times higher in the Fe-rich smectite residue. These values represent 15 and 10 % of the carbon and 9 % and 13 % of the nitrogen initially present in the starting solution containing HMT, for Al-rich smectite and Fe-rich smectite residues, respectively.

### 3.2.3 Infrared spectroscopy

#### 3.2.3.1 Mid-infrared range 3800-1000 cm<sup>-1</sup>

The starting materials from both experiments exhibit several well-defined bands, at 1237, 1374, 1462 cm<sup>-1</sup> and at 2950 cm<sup>-1</sup> (\* on Fig. 4), characteristic of the HMT (Bernstein et al., 1994). The intensities of these bands are higher in the IR spectra of the Fe-rich smectite, indicating that more HMT is retained than with the Al-rich smectite. These HMT bands are no longer observed after 31 days of experiments. Instead, new absorption bands are detected and can be attributed to different bonds: OH/NH (stretching at 3800-3000 cm<sup>-1</sup>), CH (stretching at 2700-3000 cm<sup>-1</sup>), C=O/C=N/C=C (stretching and bending at 1550-1850 cm<sup>-1</sup>), NH (bending at 1600-1400 cm<sup>-1</sup>), CH/OH (bending at 1450-1200 cm<sup>-1</sup>) and C-N/C-O (stretching at 1250-900 cm<sup>-1</sup>) (Coates, 2006). The OH band (bending at 1632 cm<sup>-1</sup>) in all spectra is attributed to free water adsorbed on phyllosilicate surfaces and to interlayer water. Bands at 3292 and 1420 cm<sup>-1</sup> in experimental residues (NH stretching and bending modes respectively) are indicative of the presence of ammonium (NH<sub>4</sub><sup>+</sup>) (Russell, 1965; Bishop et al., 2002) and present different intensities between the two smectite residues. The stretching OH of the 31-day Fe-rich smectite residue is different from that of the starting material (3527 vs 3566 cm<sup>-1</sup>), indicating a different environment around the phyllosilicate. Interestingly, the 31-day Al-rich smectite residue spectrum displays two new peaks at 3695

and  $3622\text{ cm}^{-1}$  (Fig. 5), likely corresponding to structural OH of kaolin phyllosilicates ( $\text{Al}_2\text{Si}_2\text{O}_5(\text{OH})_4$ ), such as kaolinite or dickite (Brindley et al., 1986; Prost et al., 1989).

### 3.2.3.2 Mid-far infrared range $1200\text{-}370\text{ cm}^{-1}$

Several bands in the spectral range  $1200\text{-}370\text{ cm}^{-1}$  indicate interactions at the basal or lateral edges of the phyllosilicates such as the Fe-OH (for the Fe-rich smectite) and Mg-OH (for the Al-rich smectite) absorption bands. The Si-O-Si stretching band characterizes the basal surface.

The pure Fe-rich smectite spectrum presents a Si-O-Si stretching band centered at  $969\text{ cm}^{-1}$ , and several bending modes ( $\delta$ ) characteristics of Fe or Al-OH bonds ( $865$ ,  $840$ ,  $814$  and  $784\text{ cm}^{-1}$ ) (Goodman et al., 1976; Gates, 2008). In the spectrum of the starting material, the  $\delta\text{-Fe}^{3+}\text{-OH}$  band is missing ( $838\text{ cm}^{-1}$ ) (Fig. 6-A), indicating bonding of HMT at the edge of the phyllosilicate. After 31 days, the Si-O-Si band in the spectrum of the solid Fe-rich smectite residue is shifted towards lower wavenumbers, from  $970$  to  $940\text{ cm}^{-1}$ , probably due to interactions with newly formed organic compounds.

The pure Al-rich smectite spectrum displays a Si-O-Si stretching band centered at  $990\text{ cm}^{-1}$ , an Al-OH bending band at  $915\text{ cm}^{-1}$  and a Mg-OH bending band at  $846\text{ cm}^{-1}$  (Fig. 6-B). This latter absorption is hardly observed on the residue of experiments after 31 days. Moreover, the Si-O-Si stretching band shifts to higher wavenumbers after 31 days ( $\Delta \sim 15\text{ cm}^{-1}$ ), probably due to the presence of organic compounds but potentially because of the formation of the kaolinite (Frost and Vassallo, 1996).

### 3.2.4 X-ray diffraction

The (001) reflection of the pure Fe-rich smectite is broad and shows two contributions at  $10.68$  and  $8.92^\circ$  ( $2\theta$ ), corresponding to a  $d_{001}$  of  $0.96\text{ nm}$  and  $1.13\text{ nm}$  (Fig. 7). This implies either two hydration states, the 001 interlayer distance of  $0.96\text{ nm}$  corresponding to dehydrated layers and the  $1.13\text{ nm}$  reflection corresponding to one sheet of water in the interlayer space. Such XRD signature is documented for expandable phyllosilicates made of a mixture of a high layer charge and a low layer charge (Sato et al., 1992; Decarreau et al., 2008). The starting material displays a  $d_{001}$  peak at  $6.9^\circ$  ( $2\theta$ ),  $1.49\text{ nm}$ , likely due to the intercalation of HMT. The XRD pattern of the residue after 31 days

displays a broad, composite  $d_{001}$  with two reflections at 1.10 nm and 1.27 nm, i.e. 0.14 nm, higher than those of the pure Fe-rich smectite, suggesting the incorporation of OM and likely  $\text{NH}_4^+$ , as seen by FTIR, within the interlayer spaces.

The 001 reflection of pure Al-rich smectite corresponds to an interlayer distance of 1.22 nm, typical of a  $\text{Na}^+$  saturated smectite with one intercalated water sheet (Reinholdt et al., 2001). The residues of experiments conducted in the absence of HMT shows an interlayer distance of 1.13 nm, likely due to a partial dehydration of the smectite during the washing/drying procedure. The  $d_{001}$  reflection of the starting material is broad and slightly shifted to the lower angles. This is probably due to the heterogeneity of the layer, indicating that some HMT has been intercalated, but in lower quantity than for the starting material with Fe-rich smectite. The XRD pattern of the residues after 31 days displays a  $d_{001}$  at 1.3 nm, i.e. 0.08 nm higher than those of the pure Al-rich smectite, indicating the intercalation of OM. A small peak at  $14.35\ 2\theta$  (0.71 nm) is present on the 31 days XRD pattern, likely corresponding to the  $d_{001}$  reflection of kaolin phyllosilicate (Dudek et al., 2007; Lagaly et al., 2013), in agreement with its identification by IR (Fig. 5).

### 3.2.5 STXM –XANES

STXM absorption maps on the two residues after 31 days of hydrothermal alteration, reveal that organic matter are present everywhere, in close association with smectite aggregates (Fig. 8). The high optical density measured at energies below the carbon K-edge indicate that the particles are a mixture of both smectite and organic matter. Differences in chemical speciation are observed between each smectite residue (Fig. 8). The C-XANES spectrum of the Fe-rich smectite residue displays a strong contribution of amide groups at 288.2 eV while the spectrum of the OM associated with the Al-rich smectite residue shows a strong contribution of aliphatic carbons around 287.6 eV. Both C-XANES spectra also exhibit weak peaks around 285 and 285.4 eV indicating the presence of aromatic or olefinic functional groups and imine functional groups likely within heterocycle rings. At the N-K edge, the intense absorption centered at 401.5 eV for both carbon-rich smectite particles can be explained by the presence of ammonium (Leinweber et al., 2007). Small peaks can also be observed at 398.9 and 400 eV and 401.5 eV, potentially indicating the presence of imine and/or N-heterocycle containing amine and imine groups (Leinweber et al., 2007). In comparison, the insoluble and soluble OM, formed during experiments conducted with HMT in the absence of smectite, are much richer in aromatic and N-heterocycles functional

groups (Vinogradoff et al., 2018) than the organic compounds associated with the phyllosilicates.

## 4 Discussion

### 4.1 Mutual influence of smectite and organic matter during hydrothermal evolution

In the presence of smectites at 150°C, our study reveals that HMT evolves into a diverse suite of light, nitrogen-bearing DCM soluble organic compounds as well as several organic compounds associated with smectites. Experiments performed without smectite under the same hydrothermal conditions (Vinogradoff et al., 2018) allows us to show that the presence of smectites modified organic chemical reactions. In the absence of smectite, HMT yields a wide diversity of - mainly N-rich - soluble organic compounds as well as a small amount of insoluble organic matter (Vinogradoff et al., 2018). We discussed that HMT dissociates into ammonia and formaldehyde (Meissner et al., 1954; Blažzević et al., 1979), which are afterwards involved in formose (formaldehyde condensation to form sugars) and Maillard-type reactions (reactions of sugar derivatives with amines). These reactions result in the formation of small molecules such as amines and sugars then of LC followed by their oligomerization/polymerisation into HC. The appearance of dimethylformamide also suggests the formation of some of the LC and HC by formamide condensation (Saladino et al., 2012), which is part of the Maillard reactions. Meanwhile, the most volatile species such as NH<sub>3</sub> or CH<sub>4</sub> are degassed from the solution.

Similar soluble compounds are observed in the present study in the presence of smectites, as detected on the DCM extract (Fig 3., table 1), which indicates that similar chemical reactions occur. However, the presence of smectites leads to the production of a much lower diversity of LC and HC molecules in different relative proportions as shown from the GC-MS analysis of the DCM extract (Fig. 3). Experiments conducted in the presence of smectites produced only 56 and 104 LC and HC species from the Fe-rich smectite+HMT and Al-rich smectite+HMT samples, respectively, while 150 LC and HC species are produced in the absence of smectites. The LC and HC have lower molecular masses and appear less complex and less polymerized in the presence of smectites. However, it is to note, that the GC-MS analyses were performed only on the DCM extracts and that polar compounds which are soluble in water (such as amines and sugars) are likely to be present as well. Their relative concentration might also be a function of the presence/absence as well as of the nature of the smectite. In addition, the XANES chemical

signatures of the OM tied to the smectite have specific signatures compared to the OM produced in the absence of phyllosilicates (Fig. 8). These organic compounds consist in a larger fraction of aliphatic and amide functions and a lower fraction of carbonyl, imine, aromatic functional groups, as observed by XANES (Fig. 8).

The presence of HMT also impacts the nature of the smectites. First, the interlayer spaces of both smectites are enlarged compared to the reference materials, which is likely due to the intercalation of OM. Second, the shift of some of the FTIR absorption shows that the surface bonds of smectites are modified. Both effects indicate a crystallographic and chemical influence of HMT on the composition / structure of the smectite. In addition, the formation of kaolin phyllosilicate (likely kaolinite) from Al-rich smectite is highlighted by FTIR and XRD (Fig. 5, 7) during experiments conducted with HMT, while kaolinite did not appear during the control experiments conducted in the absence of HMT. One possible pathway for kaolin phyllosilicate formation is through partial dissolution of Al-rich smectite which can occur in alkaline pH conditions (Bauer and Berger, 1998; Dudek et al., 2007; Zhang et al., 2010).

## 4.2 Mechanism of phyllosilicate(smectite)-OM interactions

### 4.2.1 Interactions at the surface

The shift of the Si-O-Si absorption band in IR and the disappearance of some of the bands attributed to cation-OH bending at the phyllosilicate edges are diagnostic of surface interactions. A fraction of the organic compounds may be sorbed onto the surface of smectites. Such sorption is driven by: 1) the intrinsic properties of smectites (charge, surface area, porosity, grain size); 2) the intrinsic properties of organic compounds (electronegativity, polarity, steric hindrance); and 3) the experimental conditions (molecule-mineral ratio, pH, temperature). Phyllosilicates have a high sorption capacity ranging from physisorption (Van Der Waals interactions, electrostatic interactions) to chemisorption (formation of a covalent bond, hydrogen bonding, coordination bonding) (Schoonen et al., 2004; Ganor et al., 2009) (Fig. 9). Chemisorption can become irreversible and thus stabilizes organic compounds (Wang and Lee, 1993; Drouin et al., 2010). Physisorption reactions (Van der Waals interactions) are reversible but can promote reactions such as peptides formation from amino acids at the montmorillonite surface, thanks to the zwitterionic nature of the amino acids (Ferris et al., 1996; Hashizume, 2012; Fuchida et al., 2014; Jaber et al., 2014). Another sorption process can occur through chelation of organic

compounds with metal ions in the solutions (Lagaly et al., 2013). This process could have been favorable for the kaolinite stabilization after Al-rich smectite dissolution, through the capture of  $Mg^{2+}$  in chelate aggregates with organic compounds.

Here, given the alkaline pH of the solution, the basal and lateral surfaces of the Al-rich and Fe-rich smectites are negatively charged ( $O^-$ ) (Fig. 9). In these conditions, organic compounds positively or neutrally charged can be adsorbed via hydrogen bonding. In our conditions, HMT mainly decomposes into ammonia (which is protonated at pH 9.2) as well as aliphatic amines ( $RNH^+$ ,  $RNH_2^+$  and  $RNH_3^+$ ) protonated around pH 10-11.5 (Perrin et al., 1981; Wang and Lee, 1993), as already reported (Vinogradoff et al., 2018). Such compounds, positively charged, may be strongly adsorbed at the surfaces of smectites or intercalated (see below), modifying their reactivity. Surface polymerization of these compounds may occur and contribute to the stabilization of the OM at the smectite surface (Lagaly et al., 2013). XANES spectra of the smectite residues show indeed the presence of aliphatic (probably amines) and amide compounds intimately associated (Fig. 8). Furthermore, neutral and polar compounds, such as alcohols, can form hydrogen bonding with the surfaces of smectites (Fig. 9) (Gabel and Ponnamparuma, 1967; Hashizume, 2012). In contrast, imines and nitrogen heterocycles are likely negatively charged at the pH of the experiments and will be less attracted by the negatively charged surface, hence remaining in the aqueous solution as identified by GC-MS (Fig. 3).

#### 4.2.2 Interactions within the interlayer space

The modification of the interlayer distances of smectites and the shifts of the IR hydroxyl stretching bands reveal that some organic molecules are trapped within their interlayer spaces. There is abundant literature on the intercalation of various organic compounds into various phyllosilicates. For instance, formamide, imidazole or potassium acetate, which are formed in our experiments, are known to intercalate within the interlayer spaces of smectites (Lagaly et al., 2013). Intercalation may result from different processes, which are impossible to distinguish in the complex system of the present experiments. One efficient intercalation process however, is the cation-exchange reactions (Schoonen et al., 2004; Lagaly et al., 2013). It involves the exchange of the cation, here  $Na^+$ , with an intercalated organic ion, a process mainly controlled by the layer charge of the mineral. Ammonium and alkylammonium cations ( $NH_4^+$  and  $RNH_3^+$ ) are known as a competitive exchangeable cations (Russell, 1965; Petit et al., 1998; Bishop et al., 2002). The presence of  $NH_4^+$

observed by FTIR spectroscopy (Fig. 4) point to cation exchange during experiments (Fig. 9). The high intensity of the  $\text{NH}_4^+$  bands (Fig. 4) and the high N/C values (table 3) of the organic compounds from the Fe-rich smectite residue can be explained by cationic exchange between  $\text{Na}^+$  and positively charged ammonia and/or N-rich organic compounds. Other mechanisms, such as regular sorption (Fig.10) could also have contributed to the intercalation of OM. Once intercalated, this OM and cations may be protected from further chemical reaction and stabilized by the smectite crystallographic structure preventing them from solvent extraction.

Altogether, the present experiments highlight the possibility of intercalation and adsorption of a large quantity of OM (3-4 wt%-table 3) within smectites at 150 °C under alkaline conditions. Such interactions undoubtedly modify the organic chemical reactions that occur in the absence of smectites (Vinogradoff et al., 2018).

### 4.3 Influence of the nature of smectites

The Al-rich and Fe-rich smectites do not have the same influence on the evolution of the OM. The residue of the experiments conducted with the Fe-rich smectite have a lower C content, a higher N/C ratio, a lower diversity of LC and HC (GC-MS), a higher amide and aromatic content (XANES), and a stronger shift of the OH vibrational modes compared to the residue from the Al-rich smectite+HMT experiment (FTIR). Both smectites have a similar mineralogical structure (2:1; Fig. 1), but they differ in chemistry, layer charge and specific surface area. Precisely identifying which of these parameters is responsible for the observed differences is challenging, but several hypotheses can be invoked. First, the different chemical composition of the smectites implies different oxidation states, as well as the release in solution of different cations through dissolution, possibly leading to the formation of different OM-rich complexes, and in turn, different catalyzing/inhibiting reactions. Second, the higher initial charge of the Fe-rich smectite, which contains 30% more Na than the Al-rich smectite, have likely promote interlayer cation exchanges (Petit et al., 2006), which is visible through the more intense IR bands of  $\text{NH}_4^+$  and XANES absorption band at 401.5 eV (Fig. 4). The Fe-rich smectite has retained more ammonium cation than the Al-rich smectite, hence possibly decreasing some chemical reactions. Since the interlayer cations contribute to the acidity of smectite surfaces (Varma, 2002), surface related reactions would be affected as well. The shift of the OH-stretching band observed by FTIR for the Fe-rich smectite residue (not observed for the Al-rich smectite residue) (Fig.

4), can be correlated to the nature of the organic cations interacting with the edges and the basal surfaces. Lastly, the Al-rich smectite has a larger specific surface than the Fe-rich smectite (table 2), potentially adsorbing more compounds and explaining the overall larger carbon content in the residue of experiments. Hence, even if relatively similar organic molecules are produced between the two smectite experiments, surface-related, chelation and intercalation reactions may be different, leading to the different chemistry observed.

#### 4.4 Implications for carbonaceous chondrites

The formation of phyllosilicates in chondrites is generally attributed to the hydrothermal events occurring within the asteroidal parent bodies (Tomeoka and Buseck, 1985; Brearley, 2006; Rubin et al., 2007). The origin and evolution of the organic matter, however, remains a delicate subject of investigations. Several studies tend to indicate that hydrothermal events have affected the molecular and physical nature of asteroidal OM (Alexander et al., 2007; Glavin et al., 2010; Cody et al., 2011; Kebukawa et al., 2013; Orthous-Daunay et al., 2013; Alexander et al., 2014; Le Guillou et al., 2014; Yabuta et al., 2017; Changela et al., 2018; Vinogradoff et al., 2018). In carbonaceous chondrites, OM occurs as individual particles as well as diffuse OM physically embedded within the phyllosilicates at the nanometer scale (Zega et al., 2010; Le Guillou et al., 2014; Le Guillou and Brearley, 2014; Vinogradoff et al., 2017; Changela et al., 2018). This association has been interpreted as the result of the formation of phyllosilicates in a fluid carrying organic compounds (Le Guillou and Brearley, 2014). The chemical signature of the diffuse OM in CC, intimately associated with phyllosilicates, is less aromatic and more carboxylic-rich than that of the individual particles (Le Guillou et al., 2014; Vinogradoff et al., 2017), which resembles the OM signature associated with the smectites in our experiments (Fig. 8). The present experimental results suggest that it could be due to specific interactions with phyllosilicates, which would have selectively retained some of the organic compounds, depending on the exact nature of the phyllosilicates and the chemistry of the fluid. This could have led to stabilization of some absorbed/trapped OM during hydrothermal alteration. In parallel, phyllosilicates have also evolved either through growth or through dissolution and precipitation of new mineral phases (Brearley, 2006). As shown here, the presence of OM may promote the destabilization of smectites and the release of cations in the fluid that could form chelates, as organic-magnesium complexes. Hence, the presence

and nature of OM during phyllosilicate formation could have guided the mineral reactions. The respective magnitude of these interactions was undoubtedly controlled by the environmental conditions (pH, temperature, water to rock ratio, organic to mineral ratio, oxygen fugacity).

Another important implication of the present results is that phyllosilicates are able to trap large amount of organic compounds, either onto their surfaces or within their interlayer spaces. We show that such compounds are not extractable, even with intense washing using water and organic solvents at room temperature. This has important implications for the study of soluble compounds in chondrites. It is indeed conceivable that a significant part of the soluble compounds of carbonaceous chondrites remains trapped within phyllosilicates during the extraction protocols. It could imply that the SOM abundance is likely underestimated; a suggestion that had been made before based on mass balance calculation (Pearson et al., 2006; Alexander et al., 2017).

Finally, the present study demonstrates that different phyllosilicates can have different effects, potentially explaining some of the chemical differences observed among chondrites. Carbonaceous chondrites contain many different (phyllo)silicates, depending on the nature of the accreted material and the intensity of the aqueous activity (Brearley, 2006). The most abundant phyllosilicates are serpentines and smectites, which display variable Fe/Mg values depending on the chondrite group and the degree of aqueous alteration. Our results indicate that Fe-rich smectites are more favorable to retaining nitrogen, possibly as ammonium ions and/or amine/amide compounds, than Al-rich smectites. Hence, the nature of the phyllosilicate plays a role and should be considered to understand the origin of chondritic OM.

## 5 Concluding remarks

This study improves our understanding of the evolution of OM in the context of asteroidal hydrothermal alteration. We show here that the chemical evolution of OM strongly depends on the presence and the nature of phyllosilicates. Compared to the transformations of HMT in the absence of phyllosilicates, a lower diversity and abundance of LC and HC compounds is observed. The adsorption and intercalation of OM hinder the molecular evolution observed otherwise. About 2-4 wt.% of carbon remain trapped within the phyllosilicates after washing. Meanwhile, the presence of OM also impacts the stability of phyllosilicates, as illustrated by the partial dissolution of the Al-rich smectite and the

formation of kaolinite. These phyllosilicate-OM interactions demonstrate the important role of hydrothermal systems while investigating the origin of the chemical complexities of organic compounds in carbonaceous chondrites and other hydrothermal systems. Noteworthy, a wide range of other phases are present in the matrix of CCs, such as serpentines, iron-oxides or sulfides and sulfates, which could potentially affect the OM as well (McCollom and Seewald, 2003; McCollom and Seewald, 2007; Yang et al., 2018). Additional investigations are required to further constrain the whole history of OM in asteroids.

Besides chondrites, this work also opens new avenues for the interpretation of the OM formation in planetary small bodies such as Ceres, which has undergone intensive hydrothermal alteration (McSween et al., 2017). Ammoniated phyllosilicates are ubiquitous at the surface of Ceres (De Sanctis et al., 2015; Ammannito et al., 2016), and their origin as well as their association with organic compounds (De Sanctis et al., 2019) could be discussed under the prism of the ability of phyllosilicates to retain large amounts of N-rich organic compounds.

## Acknowledgement

We gratefully acknowledge support from the program Emergences Ville de Paris (PI: L. Remusat), the program Emergence Sorbonne Universités (PI: S. Bernard), the MNHN ATM program (PI: V. Vinogradoff). This work was also supported by the Programme National de Planétologie (PNP) of CNRS/INSU, co-funded by CNES (PI V. Vinogradoff). We are grateful to François Baudin (ISTep, Paris) for his help with elemental analysis, Matthieu Lebon and Xavier Gallet (Plateau de spectroscopie infrarouge du MNHN, HNHP, Paris) for their help with IR spectroscopy, Christelle Anquetil and Sylvie Derenne (METIS, Paris) for their help with GC-MS, Ludovic Delbes for his help with X-ray diffraction measurements and Jessica Brest for BET analysis. We thank Jose Aponte and two anonymous referees for their thorough and constructive reviews that helped to improve this paper.

## References

- Alexander C. M. O'D., Cody G. D., De Gregorio B. T., Nittler L. R. and Stroud R. M. (2017) The nature, origin and modification of insoluble organic matter in chondrites, the major source of Earth's C and N. *Chemie der Erde - Geochemistry* **77**, 227–256.
- Alexander C. M. O'D., Cody G. D., Kebukawa Y., Bowden R., Fogel M. L., Kilcoyne A. L. D., Nittler L. R. and Herd C. D. K. (2014) Elemental, isotopic, and structural changes in Tagish Lake insoluble organic matter produced by parent body processes. *Meteoritics and Planetary Science* **49**, 503–525.
- Alexander C. M. O'D., Fogel M., Yabuta H. and Cody G. D. (2007) The origin and evolution of chondrites recorded in the elemental and isotopic compositions of their macromolecular organic matter. *Geochimica et Cosmochimica Acta* **71**, 4380–4403.
- Alexander C. M. O'D., Hutchison R. and Barber D. J. (1989) Origin of chondrule rims and interchondrule matrices in unequilibrated ordinary chondrites. *Earth and Planetary Science Letters* **95**, 187–207.
- Allamandola L. J., Sandford S. A. and Valero G. J. (1988) Photochemical and thermal evolution of interstellar/precometary ice analogs. *Icarus* **76**, 225–252.
- Ammannito E., DeSanctis M. C., Ciarniello M., Frigeri A., Carrozzo F. G., Combe J.-P., Ehlmann B. L., Marchi S., McSween H. Y., Raponi A., Toplis M. J., Tosi F., Castillo-Rogez J. C., Capaccioni F., Capria M. T., Fonte S., Giardino M., Jaumann R., Longobardo A., Joy S. P., Magni G., McCord T. B., McFadden L. A., Palomba E., Pieters C. M., Polanskey C. A., Rayman M. D., Raymond C. A., Schenk P. M., Zambon F. and Russell C. T. (2016) Distribution of phyllosilicates on the surface of Ceres. *Science* **353**, aaf4279.
- Andrieux P. and Petit S. (2010) Hydrothermal synthesis of dioctahedral smectites: The Al–Fe<sup>3+</sup> chemical series: Part I: Influence of experimental conditions. *Applied Clay Science* **48**, 5–17.
- Aponte J. C., McLain H. L., Dworkin J. P. and Elsila J. E. (2016) Aliphatic amines in Antarctic CR2, CM2, and CM1/2 carbonaceous chondrites. *Geochimica et Cosmochimica Acta* **189**, 296–311.
- Bauer A. and Berger G. (1998) Kaolinite and smectite dissolution rate in high molar KOH solutions at 35° and 80°C. *Applied Geochemistry* **13**, 905–916.
- Beck P., Quirico E., Montes-Hernandez G., Bonal L., Bollard J., Orthous-Daunay F.-R., Howard K. T., Schmitt B., Brissaud O., Deschamps F., Wunder B. and Guillot S. (2010) Hydrous mineralogy of CM and CI chondrites from infrared spectroscopy and their relationship with low albedo asteroids. *Geochimica et Cosmochimica Acta* **74**, 4881–4892.
- Bernstein M. P., Sandford S. A., Allamandola L. J. and Chang S. (1994) Infrared Spectrum of Matrix-Isolated Hexamethylenetetramine in Ar and H<sub>2</sub>O at Cryogenic Temperatures. *J. Phys. Chem.* **98**, 12206–12210.
- Bernstein M. P., Sandford S. A., Allamandola L. J., Chang S. and Scharberg M. A. (1995) Organic Compounds Produced by Photolysis of Realistic Interstellar and Cometary Ice Analogs Containing Methanol. *The Astrophysical Journal* **454**, 327.

- Bishop J. L., Banin A., Mancinelli R. L. and Klovstad M. R. (2002) Detection of soluble and fixed NH<sub>4</sub><sup>+</sup> in clay minerals by DTA and IR reflectance spectroscopy: a potential tool for planetary surface exploration. *Planetary and Space Science* **50**, 11–19.
- Blažzević N., Kolbah D., Belin B., Šunjić V. and Kajfež F. (1979) Hexamethylenetetramine, A Versatile Reagent in Organic Synthesis. *Synthesis* **3**, 161–176.
- Brearley A. J. (2006) The Action of Water. In *Meteorites and the Early Solar System II* pp. 584–624. Available at: <http://adsabs.harvard.edu/abs/2006mess.book..584B> [Accessed October 25, 2016].
- Brindley G. W., Kao C., Harrison J. L., Lipsicas M. and Raythatha R. (1986) Relation between the structural disorder and other characteristics of kaolinites and dickites. *Clays and Clay Minerals*, 233–249.
- Busemann H., Young A. F., Alexander C. M. O'D., Hoppe P., Mukhopadhyay S. and Nittler L. R. (2006) Interstellar Chemistry Recorded in Organic Matter from Primitive Meteorites. *Science* **312**, 727–730.
- Caselli P. and Ceccarelli C. (2012) Our astrochemical heritage. *Astron Astrophys Rev* **20**, 56.
- Changela H. G., Guillou C. L., Bernard S. and Brearley A. J. (2018) Hydrothermal evolution of the morphology, molecular composition, and distribution of organic matter in CR (Renazzo-type) chondrites. *Meteoritics & Planetary Science* **53**, 1006–1029.
- Coates J. (2006) Interpretation of Infrared Spectra, A Practical Approach. In *Encyclopedia of Analytical Chemistry* John Wiley & Sons, Ltd. Available at: <http://onlinelibrary.wiley.com/doi/10.1002/9780470027318.a5606/abstract> [Accessed January 13, 2017].
- Cody G. D., Heying E., Alexander C. M. O'D., Nittler L. R., Kilcoyne A. L. D., Sandford S. A. and Stroud R. M. (2011) Establishing a molecular relationship between chondritic and cometary organic solids. *PNAS* **108**, 19171–19176.
- Connolly M. L. (1983) Solvent-accessible surfaces of proteins and nucleic acids. *Science* **221**, 709–713.
- Danger G., Orthous-Daunay F.-R., de Marcellus P., Modica P., Vuitton V., Duvernay F., Flandinet L., Le Sergeant d'Hendecourt L., Thissen R. and Chiavassa T. (2013) Characterization of laboratory analogs of interstellar/cometary organic residues using very high resolution mass spectrometry. *Geochimica et Cosmochimica Acta* **118**, 184–201.
- De Gregorio B. T. D., Stroud R. M., Nittler L. R., Alexander C. M. O'D., Bassim N. D., Cody G. D., Kilcoyne A. L. D., Sandford S. A., Milam S. N., Nuevo M. and Zega T. J. (2013) Isotopic and chemical variation of organic nanoglobules in primitive meteorites. *Meteoritics & Planetary Science* **48**, 904–928.

- De Sanctis M. C., Ammannito E., Raponi A., Marchi S., McCord T. B., McSween H. Y., Capaccioni F., Capria M. T., Carrozzo F. G., Ciarniello M., Longobardo A., Tosi F., Fonte S., Formisano M., Frigeri A., Giardino M., Magni G., Palomba E., Turrini D., Zambon F., Combe J.-P., Feldman W., Jaumann R., McFadden L. A., Pieters C. M., Prettyman T., Toplis M., Raymond C. A. and Russell C. T. (2015) Ammoniated phyllosilicates with a likely outer Solar System origin on (1) Ceres. *Nature* **528**, 241–244.
- De Sanctis M. C., Vinogradoff V., Raponi A., Ammannito E., Ciarniello M., Carrozzo F. G., De Angelis S., Raymond C. A. and Russell C. T. (2019) Characteristics of organic matter on Ceres from VIR/Dawn high spatial resolution spectra. *Mon Not R Astron Soc* **482**, 2407–2421.
- Decarreau A., Petit S., Martin F., Farges F., Vieillard P. and Joussein E. (2008) Hydrothermal synthesis between 75 and 150 °C of high-charge ferric nontronites. *Clays and Clay Minerals* **56**, 322–337.
- Derenne S. and Robert F. (2010) Model of molecular structure of the insoluble organic matter isolated from Murchison meteorite. *Meteoritics and Planetary Science* **45**, 1461–1475.
- Drouin S., Boussafir M., Robert J.-L., Alberic P. and Durand A. (2010) Carboxylic acid sorption on synthetic clays in sea water: In vitro experiments and implications for organo-clay behaviour under marine conditions. *Organic Geochemistry* **41**, 192–199.
- Dudek T., Cuadros J. and Huertas J. (2007) Structure of mixed-layer kaolinite-smectite and smectite-to-kaolinite transformation mechanism from synthesis experiments. *American Mineralogist* **92**, 179–192.
- Elsila J. E., Aponte J. C., Blackmond D. G., Burton A. S., Dworkin J. P. and Glavin D. P. (2016) Meteoritic Amino Acids: Diversity in Compositions Reflects Parent Body Histories. *ACS Cent. Sci.* **2**, 370–379.
- Ferris J. P., Hill Jr A. R., Liu R. and Orgel L. E. (1996) Synthesis of long prebiotic oligomers on mineral surfaces. *Nature* **381**, 59–61.
- Frost R. L. and Vassallo A. M. (1996) The Dehydroxylation of the Kaolinite Clay Minerals Using Infrared Emission Spectroscopy. *Clays and Clay Minerals* **44**, 635–651.
- Fuchida S., Masuda H. and Shinoda K. (2014) Peptide Formation Mechanism on Montmorillonite Under Thermal Conditions. *Orig Life Evol Biosph* **44**, 13–28.
- Gabel N. W. and Ponnampereuma C. (1967) Model for origin of monosaccharides. *Nature* **216**, 453.
- Ganor J., Reznik I. J. and Rosenberg Y. O. (2009) Organics in Water-Rock Interactions. *Reviews in Mineralogy and Geochemistry* **70**, 259–369.
- Garvie L. A. J. and Buseck P. R. (2007) Prebiotic carbon in clays from Orgueil and Ivuna (CI), and Tagish Lake (C2 ungrouped) meteorites. *Meteoritics & Planetary Science* **42**, 2111–2117.

- Gates W. P. (2008) CATION MASS-VALENCE SUM (CM-VS) APPROACH TO ASSIGNING OH-BENDING BANDS IN DIOCTAHEDRAL SMECTITES. *Clays and Clay Minerals* **56**, 10–22.
- Glavin D. P., Callahan M. P., Dworkin J. P. and Elsila J. E. (2010) The effects of parent body processes on amino acids in carbonaceous chondrites. *Meteoritics & Planetary Science* **45**, 1948–1972.
- Glavin D. P., Elsila J. E., Burton A. S., Callahan M. P., Dworkin J. P., Hilts R. W. and Herd C. D. K. (2012) Unusual nonterrestrial l-proteinogenic amino acid excesses in the Tagish Lake meteorite. *Meteoritics & Planetary Science* **47**, 1347–1364.
- Goodman B. A., Russell J. D., Fraser A. R. and Woodhams F. W. D. (1976) A Moessbauer and I.R. spectroscopic study of the structure of nontronite. *Clays and Clay Minerals* **24**, 53–59.
- Gudipati M. S., Abou Mrad N., Blum J., Charnley S. B., Chiavassa T., Cordiner M. A., Mousis O., Danger G., Duvernay F., Gundlach B., Hartogh P., Marboeuf U., Simonia I., Simonia T., Theulé P. and Yang R. (2015) Laboratory Studies Towards Understanding Comets. *Space Sci Rev* **197**, 101–150.
- Hashizume H. (2012) Role of clay minerals in chemical evolution and the origins of life. In *Clay Minerals in Nature-Their Characterization, Modification and Application* IntechOpen.
- Herd C. D. K., Blinova A., Simkus D. N., Huang Y., Tarozo R., Alexander C. M. O'D., Gyngard F., Nittler L. R., Cody G. D., Fogel M. L., Kebukawa Y., Kilcoyne A. L. D., Hilts R. W., Slater G. F., Glavin D. P., Dworkin J. P., Callahan M. P., Elsila J. E., Gregorio B. T. D. and Stroud R. M. (2011) Origin and Evolution of Prebiotic Organic Matter As Inferred from the Tagish Lake Meteorite. *Science* **332**, 1304–1307.
- Hilts R. W., Herd C. D. K., Simkus D. N. and Slater G. F. (2014) Soluble organic compounds in the Tagish Lake meteorite. *Meteoritics & Planetary Science* **49**, 526–549.
- Howard K. T., Benedix G. K., Bland P. A. and Cressey G. (2011) Modal mineralogy of CM chondrites by X-ray diffraction (PSD-XRD): Part 2. Degree, nature and settings of aqueous alteration. *Geochimica et Cosmochimica Acta* **75**, 2735–2751.
- Jaber M., Georgelin T., Bazzi H., Costa-Torro F., Lambert J.-F., Bolbach G. and Clodic G. (2014) Selectivities in Adsorption and Peptidic Condensation in the (Arginine and Glutamic Acid)/Montmorillonite Clay System. *J. Phys. Chem. C* **118**, 25447–25455.
- Kebukawa Y., Chan Q. H. S., Tachibana S., Kobayashi K. and Zolensky M. E. (2017) One-pot synthesis of amino acid precursors with insoluble organic matter in planetesimals with aqueous activity. *Science Advances* **3**, e1602093.
- Kebukawa Y., Kilcoyne A. L. D. and Cody G. D. (2013) Exploring the Potential Formation of Organic Solids in Chondrites and Comets through Polymerization of Interstellar Formaldehyde. *ApJ* **771**, 19.

- Lagaly G., Ogawa M. and Dékány I. (2013) Chapter 10.3 - Clay Mineral–Organic Interactions. In *Developments in Clay Science* (eds. F. Bergaya and Gerhard Lagaly). Handbook of Clay Science. Elsevier. pp. 435–505. Available at: <http://www.sciencedirect.com/science/article/pii/B9780080982588000158> [Accessed March 8, 2019].
- Le Guillou C., Bernard S., Brearley A. J. and Remusat L. (2014) Evolution of organic matter in Orgueil, Murchison and Renazzo during parent body aqueous alteration: In situ investigations. *Geochimica et Cosmochimica Acta* **131**, 368–392.
- Le Guillou C., Bernard S., De la Pena F. and Le Brech Y. (2018) XANES-Based Quantification of Carbon Functional Group Concentrations. *Anal. Chem.* **90**, 8379–8386.
- Le Guillou C. and Brearley A. (2014) Relationships between organics, water and early stages of aqueous alteration in the pristine CR3.0 chondrite MET 00426. *Geochimica et Cosmochimica Acta* **131**, 344–367.
- Le Guillou C., Changela H. G. and Brearley A. J. (2015) Widespread oxidized and hydrated amorphous silicates in CR chondrites matrices: Implications for alteration conditions and H<sub>2</sub> degassing of asteroids. *Earth and Planetary Science Letters* **420**, 162–173.
- Leinweber P., Kruse J., Walley F. L., Gillespie A., Eckhardt K.-U., Blyth R. I. R. and Regier T. (2007) Nitrogen K-edge XANES – an overview of reference compounds used to identify ‘unknown’ organic nitrogen in environmental samples. *Journal of Synchrotron Radiation* **14**, 500–511.
- McCollom T. M. and Seewald J. S. (2007) Abiotic Synthesis of Organic Compounds in Deep-Sea Hydrothermal Environments. *Chem. Rev.* **107**, 382–401.
- McCollom T. M. and Seewald J. S. (2003) Experimental constraints on the hydrothermal reactivity of organic acids and acid anions: I. Formic acid and formate. *Geochimica et Cosmochimica Acta* **67**, 3625–3644.
- McSween H. Y., Emery J. P., Rivkin A. S., Toplis M. J., C. Castillo-Rogez J., Prettyman T. H., De Sanctis M. C., Pieters C. M., Raymond C. A. and Russell C. T. (2017) Carbonaceous chondrites as analogs for the composition and alteration of Ceres. *Meteorit Planet Sci*, 1–12.
- Meissner F., Schwiedessen E. and Othmer D. F. (1954) Continuous Production of Hexamethylenetetramine. *Ind. Eng. Chem.* **46**, 724–727.
- Montgomery W., Tuff J., Kohn S. C. and Jones R. L. (2011) Reactions between organic acids and montmorillonite clay under Earth-forming conditions. *Chemical Geology* **283**, 171–176.
- Muñoz Caro G. M. and Schutte W. A. (2003) UV-photoprocessing of interstellar ice analogs: New infrared spectroscopic results. *Astronomy & Astrophysics* **412**, 121–132.

- Orthous-Daunay F.-R., Quirico E., Beck P., Brissaud O., Dartois E., Pino T. and Schmitt B. (2013) Mid-infrared study of the molecular structure variability of insoluble organic matter from primitive chondrites. *Icarus* **223**, 534–543.
- Pearson V. K., Sephton M. A., Franchi I. A., Gibson J. M. and Gilmour I. (2006) Carbon and nitrogen in carbonaceous chondrites: Elemental abundances and stable isotopic compositions. *Meteoritics and Planetary Science* **41**, 1899–1918.
- Perrin D. D., Dempsey B. and Serjeant E. P. (1981) Methods of pKa Prediction. In *pKa Prediction for Organic Acids and Bases* (eds. D. D. Perrin, B. Dempsey, and E. P. Serjeant). Springer Netherlands, Dordrecht. pp. 21–26. Available at: [https://doi.org/10.1007/978-94-009-5883-8\\_3](https://doi.org/10.1007/978-94-009-5883-8_3) [Accessed March 8, 2019].
- Petit S., Righi D. and Madejova J. (2006) Infrared spectroscopy of NH<sub>4</sub><sup>+</sup>-bearing and saturated clay minerals: A review of the study of layer charge. *Applied Clay Science* **34**, 22–30.
- Petit S., Righi D., Madejova J. and Decarreau A. (1998) Layer charge estimation of smectites using infrared spectroscopy. *Clay Minerals* **33**, 579–591.
- Pizzarello S., Cooper G. W. and Flynn G. J. (2006) The Nature and Distribution of the Organic Material in Carbonaceous Chondrites and Interplanetary Dust Particles. In *Meteorites and the Early Solar System II* pp. 625–651. Available at: <http://adsabs.harvard.edu/abs/2006mess.book..625P> [Accessed October 25, 2016].
- Poch O., Jaber M., Stalport F., Nowak S., Georgelin T., Lambert J.-F., Szopa C. and Coll P. (2015) Effect of Nontronite Smectite Clay on the Chemical Evolution of Several Organic Molecules under Simulated Martian Surface Ultraviolet Radiation Conditions. *Astrobiology* **15**, 221–237.
- Prost R., Dameme A., Huard E., Driard J. and Leydecker J. P. (1989) Infrared Study of Structural OH in Kaolinite, Dickite, Nacrite, and Poorly Crystalline Kaolinite at 5 to 600 K. *Clays Clay Miner.* **37**, 464–468.
- Reinholdt M., Miehé- Brendlé J., Delmotte L., Tuilier M.-H., le Dred R., Cortès R. and Flank A.-M. (2001) Fluorine Route Synthesis of Montmorillonites Containing Mg or Zn and Characterization by XRD, Thermal Analysis, MAS NMR, and EXAFS Spectroscopy. *European Journal of Inorganic Chemistry* **2001**, 2831–2841.
- Remusat L. (2016) Organics in primitive meteorites. *EMU notes in Mineralogy* **15**, 1–33.
- Remusat L., Derenne S. and Robert F. (2005) New insight on aliphatic linkages in the macromolecular organic fraction of Orgueil and Murchison meteorites through ruthenium tetroxide oxidation. *Geochimica et Cosmochimica Acta* **69**, 4377–4386.
- Robert F. and Epstein S. (1982) The concentration and isotopic composition of hydrogen, carbon and nitrogen in carbonaceous meteorites. *Geochimica et Cosmochimica Acta* **46**, 81–95.
- Rubin A. E., Trigo-Rodríguez J. M., Huber H. and Wasson J. T. (2007) Progressive aqueous alteration of CM carbonaceous chondrites. *Geochimica et Cosmochimica Acta* **71**, 2361–2382.

- Russell J. D. (1965) Infra-red study of the reactions of ammonia with montmorillonite and saponite. *Trans. Faraday Soc.* **61**, 2284–2294.
- Saladino R., Botta G., Pino S., Costanzo G. and Di Mauro E. (2012) Genetics first or metabolism first? The formamide clue. *Chemical Society Reviews* **41**, 5526–5565.
- Saladino R., Neri V. and Crestini C. (2010) Role of clays in the prebiotic synthesis of sugar derivatives from formamide. *Philosophical Magazine* **90**, 2329–2337.
- Sato T., Watanabe T. and Otsuka R. (1992) Effects of layer charge, charge location, and energy change on expansion properties of dioctahedral smectites. *Clays and Clay Minerals* **40**, 103–113.
- Schoonen M., Smirnov A. and Cohn C. (2004) A Perspective on the Role of Minerals in Prebiotic Synthesis. *AMBIO: A Journal of the Human Environment* **33**, 539–551.
- Sephton M. A. (2014) 12.1 - Organic Geochemistry of Meteorites. In *Treatise on Geochemistry (Second Edition)* (eds. H. D. Holland and K. K. Turekian). Elsevier, Oxford. pp. 1–31. Available at: <http://www.sciencedirect.com/science/article/pii/B9780080959757010020> [Accessed August 28, 2019].
- Sephton M. A., Love G. D., Watson J. S., Verchovsky A. B., Wright I. P., Snape C. E. and Gilmour I. (2004) Hydrolysis of insoluble carbonaceous matter in the Murchison meteorite: new insights into its macromolecular structure. Associate editor: G. D. Cody. *Geochimica et Cosmochimica Acta* **68**, 1385–1393.
- Sephton M. A., Pillinger C. T. and Gilmour I. (2000) Aromatic moieties in meteoritic macromolecular materials: analyses by hydrous pyrolysis and  $\delta^{13}\text{C}$  of individual compounds. *Geochimica et Cosmochimica Acta* **64**, 321–328.
- Tomeoka K. and Buseck P. R. (1985) Indicators of aqueous alteration in CM carbonaceous chondrites: Microtextures of a layered mineral containing Fe, S, O and Ni. *Geochimica et Cosmochimica Acta* **49**, 2149–2163.
- Varma R. S. (2002) Clay and clay-supported reagents in organic synthesis. *Tetrahedron* **58**, 1235–1255.
- Vinogradoff V., Bernard S., Le Guillou C. and Remusat L. (2018) Evolution of interstellar organic compounds under asteroidal hydrothermal conditions. *Icarus* **305**, 358–370.
- Vinogradoff V., Duvernay F., Danger G., Theulé P. and Chiavassa T. (2011) New insight into the formation of hexamethylenetetramine (HMT) in interstellar and cometary ice analogs. *A&A* **530**, A128.
- Vinogradoff V., Duvernay F., Fray N., Bouilloud M., Chiavassa T. and Cottin H. (2015) Carbon Dioxide Influence on the Thermal Formation of Complex Organic Molecules in Interstellar Ice Analogs. *ApJL* **809**, L18.
- Vinogradoff V., Fray N., Duvernay F., Briani G., Danger G., Cottin H., Theulé P. and Chiavassa T. (2013) Importance of thermal reactivity for hexamethylenetetramine formation from simulated interstellar ices. *Astronomy & Astrophysics* **551**, A128.

- Vinogradoff V., Le Guillou C., Bernard S., Binet L., Cartigny P., Brearley A. J. and Remusat L. (2017) Paris vs. Murchison: Impact of hydrothermal alteration on organic matter in CM chondrites. *Geochimica et Cosmochimica Acta*. Available at: <http://www.sciencedirect.com/science/article/pii/S0016703717303587>.
- Vinogradoff V., Rimola A., Duvernay F., Danger G., Theulé P. and Chiavassa T. (2012) The mechanism of hexamethylenetetramine (HMT) formation in the solid state at low temperature. *Phys. Chem. Chem. Phys.* **14**, 12309–12320.
- Vollmer C., Kepaptsoglou D., Leitner J., Busemann H., Spring N. H., Ramasse Q. M., Hoppe P. and Nittler L. R. (2014) Fluid-induced organic synthesis in the solar nebula recorded in extraterrestrial dust from meteorites. *PNAS* **111**, 15338–15343.
- Wang X. and Lee C. (1993) Adsorption and desorption of aliphatic amines, amino acids and acetate by clay minerals and marine sediments. *Marine Chemistry* **44**, 1–23.
- Watson J. S. and Sephton M. A. (2015) Heat, Aromatic Units, and Iron-Rich Phyllosilicates: A Mechanism for Making Macromolecules in the Early Solar System. *Astrobiology* **15**, 787–792.
- Williams L. B., Canfield B., Voglesonger K. M. and Holloway J. R. (2005) Organic molecules formed in a “primordial womb.” *Geology* **33**, 913–916.
- Yabuta H., Noguchi T., Itoh S., Nakamura T., Miyake A., Tsujimoto S., Ohashi N., Sakamoto N., Hashiguchi M., Abe K., Okubo A., David Kilcoyne A. L., Tachibana S., Okazaki R., Terada K., Ebihara M. and Nagahara H. (2017) Formation of an Ultracarbonaceous Antarctic Micrometeorite through Minimal Aqueous Alteration in a Small Porous Icy Body. *Geochimica et Cosmochimica Acta*. Available at: <http://www.sciencedirect.com/science/article/pii/S0016703717304064>.
- Yang Z., Gould I. R., Williams L. B., Hartnett H. E. and Shock E. L. (2018) Effects of iron-containing minerals on hydrothermal reactions of ketones. *Geochimica et Cosmochimica Acta* **223**, 107–126.
- Zega T. J., Alexander C. M. O'D., Busemann H., Nittler L. R., Hoppe P., Stroud R. M. and Young A. F. (2010) Mineral associations and character of isotopically anomalous organic material in the Tagish Lake carbonaceous chondrite. *Geochimica et Cosmochimica Acta* **74**, 5966–5983.
- Zhang D., Zhou C.-H., Lin C.-X., Tong D.-S. and Yu W.-H. (2010) Synthesis of clay minerals. *Applied Clay Science* **50**, 1–11.

Figures captions

Figure 1: Schematic representation of the two synthetic phyllosilicates used in this study; A) Al-rich smectite with  $Mg^{2+}$  and  $Al^{3+}$  in the octahedral (O) layer; B) Fe-rich smectite with  $Fe^{3+}$ ,  $Mg^{2+}$  and  $Al^{3+}$  in the octahedral layer. The tetrahedral (T) layer contains the Si-O structure of smectite. Both phyllosilicates have  $Na^+$  as interlayer cation surrounded by water molecules.

Figure 2: Schematic representation of the analytical strategy followed in this study.

Figure 3: Chromatograms of the DCM extract of the solution after 31 days of experiments. Peaks are distinguished in two groups, between 5-25 min (called LC for light compounds) and after 25 min (called HC for heavy compounds). The numbered peaks are those that could be assigned to known molecules (table 1). Stars (\*) indicate GC-MS column contaminations.

Figure 4: Infrared spectra between  $3800$  and  $1000\text{ cm}^{-1}$ , normalized to their total absorbance area. Absorption bands of OM are indicated ( $\nu$  : stretching,  $\delta$  : bending). The absorption bands characteristic of HMT are highlighted with an asterisk (\*), while the shifts and the  $\nu(OH)$  band are underlined by a hash (#).

Figure 5: Infrared spectra of the Al-rich smectite series in the range  $3750$ - $3200\text{ cm}^{-1}$ , normalized to the absorbance area. The OH stretching mode of the hydroxyl groups at  $3633\text{ cm}^{-1}$  corresponds to Al-rich smectite and bands at  $3695$  and  $3622\text{ cm}^{-1}$  are indicative of kaolinite.

Figure 6: Infrared spectra between  $1200$  and  $370\text{ cm}^{-1}$  ( $\nu$  : stretching,  $\delta$  : bending) normalized to their total absorbance area. The shift of the  $\nu Si-O-Si$  band and the disappearance of some Fe-OH or Mg-OH bands may indicate adsorption of OM at the edges of the phyllosilicates.

Figure 7: XRD patterns between 4 and 15° (2 $\theta$ ) of the pure smectites, the starting materials and the solid residues of the experiments. Number refer to  $d_{001}$  in nm (+/- 0.005 nm).

Figure 8: STXM-based XANES data of carbon-rich smectite particles within solid residues of experiments after 31 days of hydrothermal alteration. On the top, differential absorption map between 288.1 eV (maximum of carbon absorption) and 280 eV (no carbon absorption, only silicate background absorption occurs) showing the distribution of organic matter (in blue) and phyllosilicate (in red). On the bottom, A: C-K edge and B: N-K edge XANES spectra of the residues from Al-rich smectite+HMT and Fe-rich smectite+HMT experiments. The XANES spectra of the IOM and SOM formed from HMT during experiments conducted in the absence of smectite are shown for comparison (Vinogradoff et al., 2018)

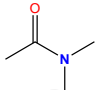
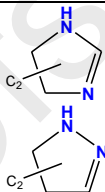
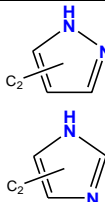
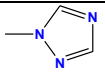
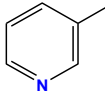
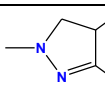
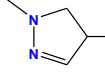
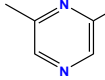
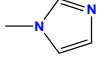
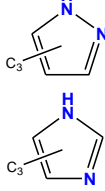
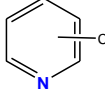
Figure 9: Illustration of the possible OM sorption mechanisms, i.e. onto the surface of Fe-rich smectite and within their interlayer spaces: physisorption, chemisorption, chelation, cationic exchange and sorption (intercalation) of OM in the interlayer space. The surfaces of smectites are negatively charged under the pH conditions of the present experiments.

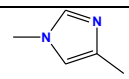
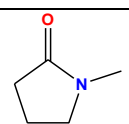
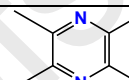
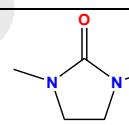
## Tables captions

Table 1: Nature of the organic molecules identified on the DCM extract of the soluble compounds after 31 days of experiments (Fig. 3). For each peak, the retention time, the molecular ion ( $m/z$ ), and their possible assignments are reported, as well as structures of molecules.

Table 2: Specific surface area of the initial Fe-rich smectite and Al-rich smectite powders and corresponding ratio of the HMT molecules at the surface of the phyllosilicate in the beginning of our experimental conditions.

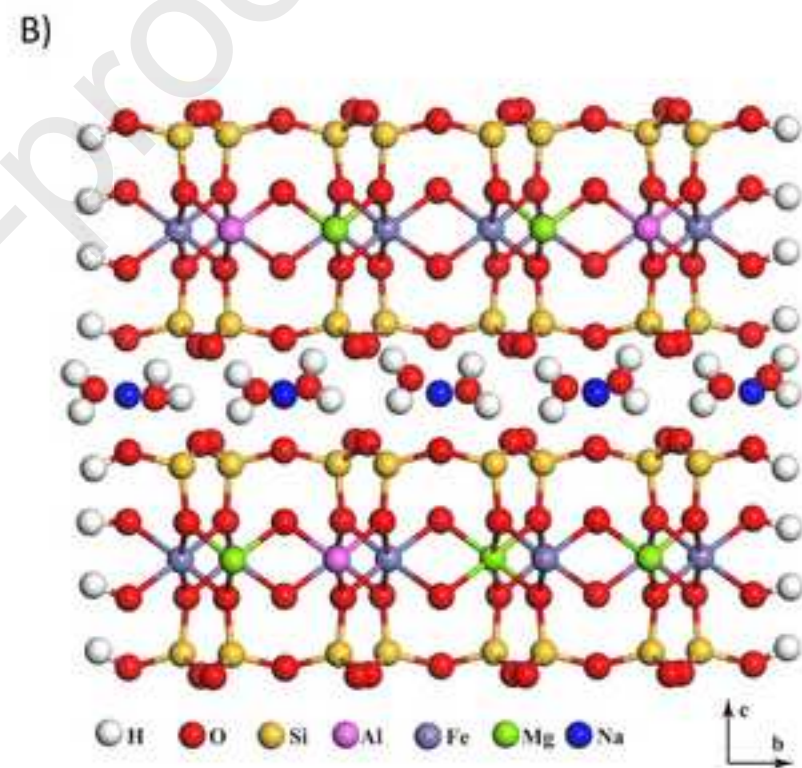
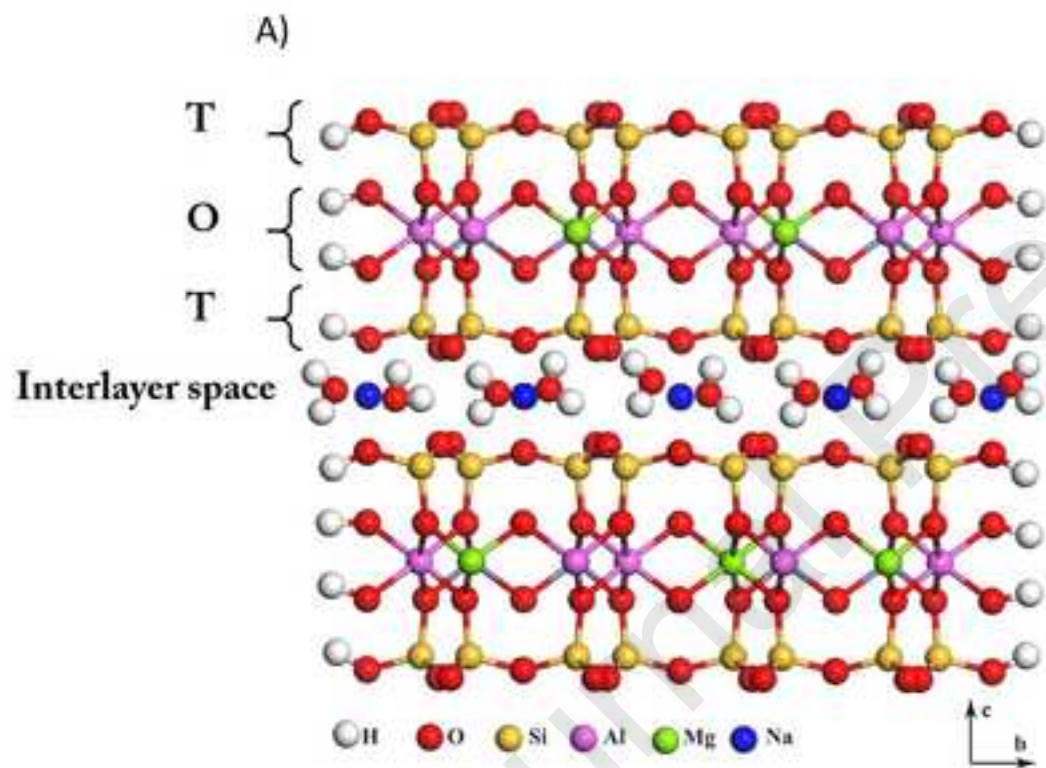
Table 3: C, N composition (wt.%) of the solid residues after 31 days of experiments.

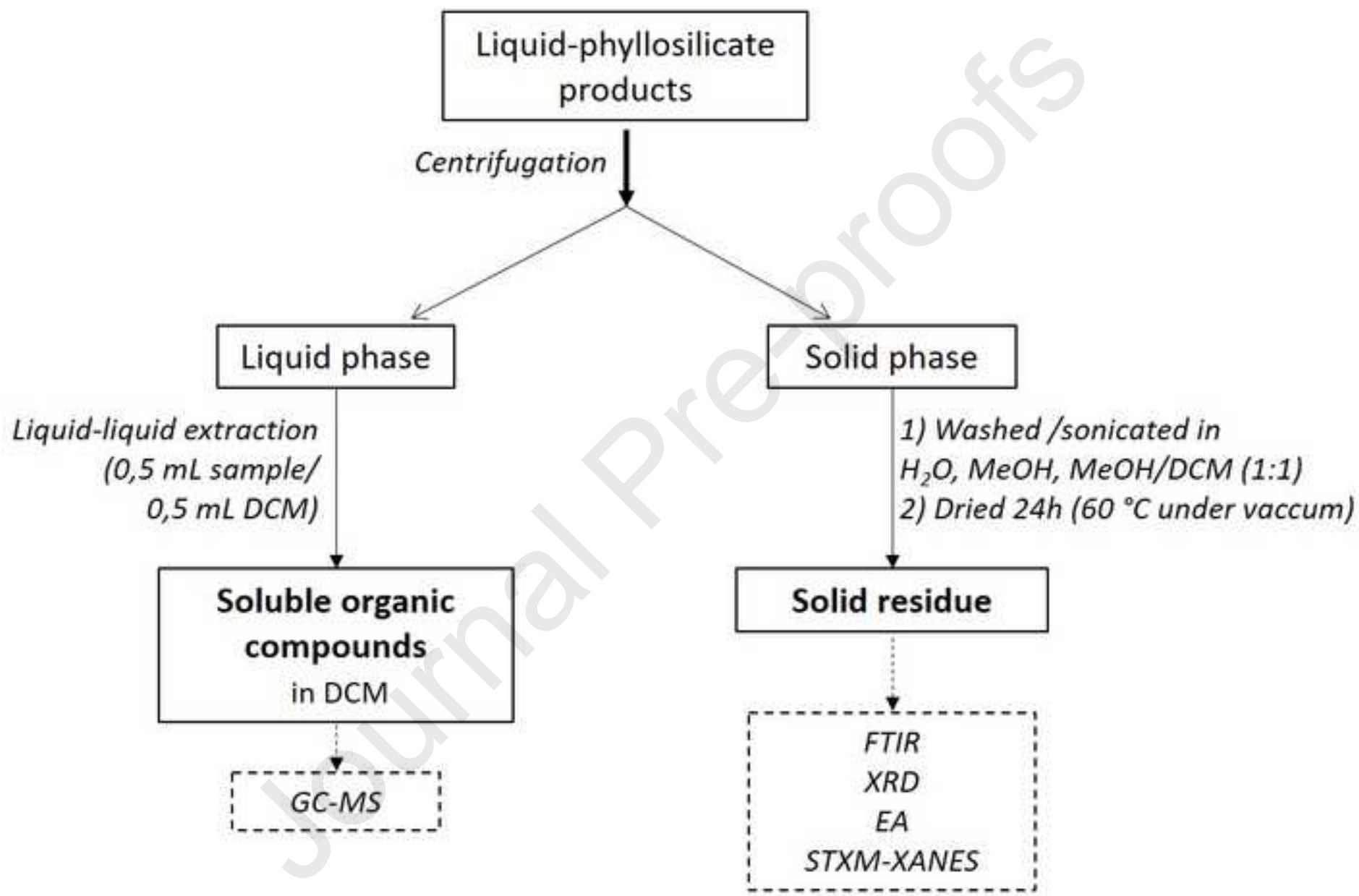
Number	Retention time	[M+] <i>m/z</i>	Possible assignment		
			Name	Formula	structures
1	5.37	73	N-N-dimethyl formamide	C <sub>3</sub> H <sub>7</sub> NO	
2	6.18	98	C2-methyl, 2-pyrazoline/imidazoline	C <sub>5</sub> H <sub>10</sub> N <sub>2</sub>	
3	6.65	96	C2-alkyl pyrazole or imidazole	C <sub>5</sub> H <sub>8</sub> N <sub>2</sub>	
4	6.94	83	1-methyl-1H-1,2,4-triazole	C <sub>3</sub> H <sub>5</sub> N <sub>3</sub>	
5	7.48	93	Pyridine, 3-methyl	C <sub>6</sub> H <sub>7</sub> N	
6	7.56	96	C2-alkyl imidazole or pyrazole	C <sub>5</sub> H <sub>8</sub> N <sub>2</sub>	See 3
7	7.82	112	2-Pyrazoline, 1,3,4-trimethyl-	C <sub>6</sub> H <sub>12</sub> N <sub>2</sub>	
8	8.73	112	2-Pyrazoline, 3-ethyl,1-methyl	C <sub>6</sub> H <sub>12</sub> N <sub>2</sub>	
9	9.07	108	Pyrazine, 2,6-dimethyl	C <sub>6</sub> H <sub>8</sub> N <sub>2</sub>	
10	9.22	82	1H-imidazole, 1-methyl	C <sub>4</sub> H <sub>6</sub> N <sub>2</sub>	
11	9.39	110	C3-alkyl imidazole or pyrazole	C <sub>6</sub> H <sub>10</sub> N <sub>2</sub>	
12	10.10	107	C2-alkyl pyridine	C <sub>7</sub> H <sub>9</sub> N	
13	10.18	110	C3-alkyl imidazole or pyrazole	C <sub>6</sub> H <sub>10</sub> N <sub>2</sub>	See 11

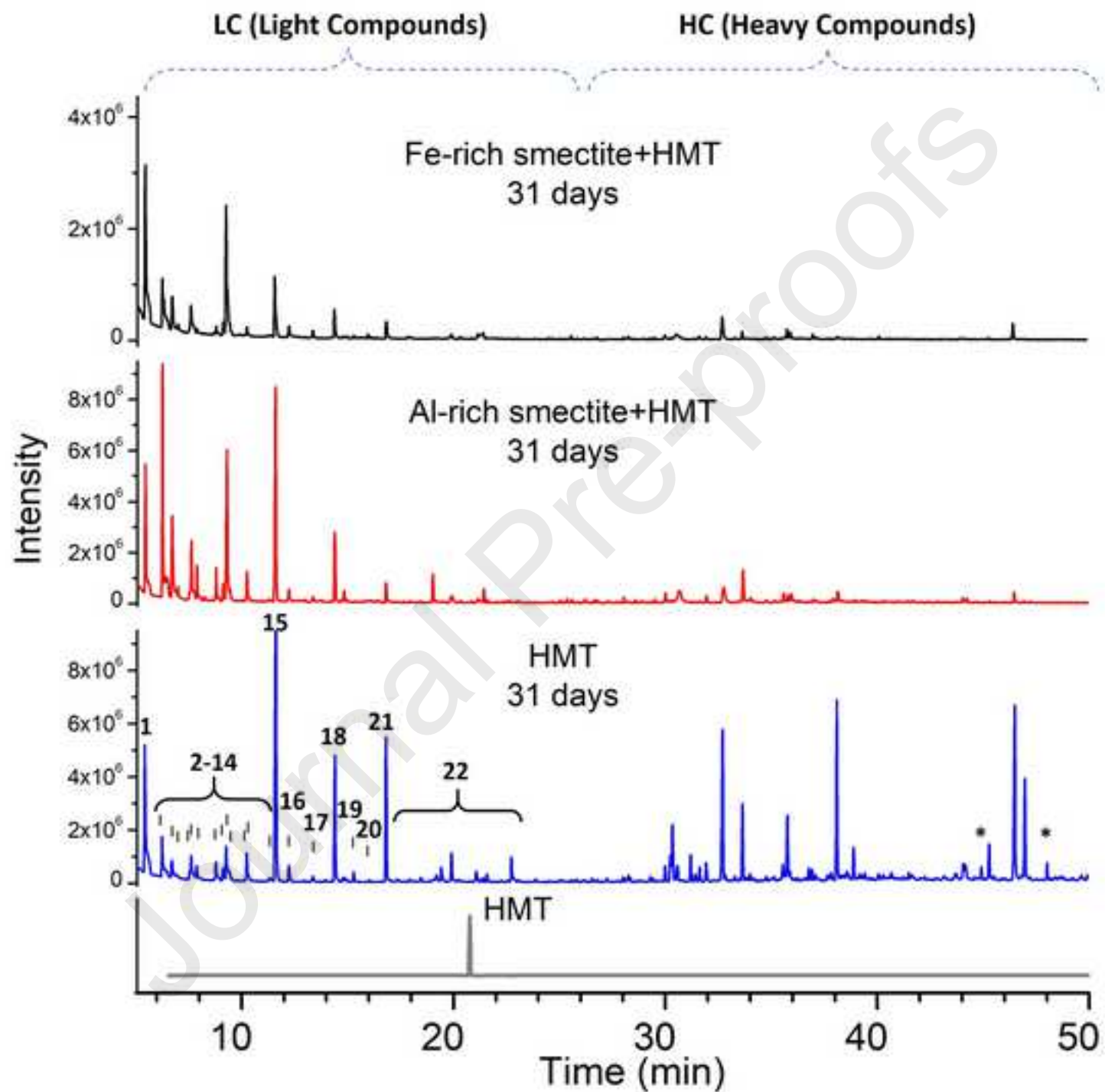
14	11.28	107	C2-alkyl pyridine	$C_7H_9N$	See 12
15	11.55	96	Imidazole-1,4-dimethyl	$C_5H_8N_2$	
16	12.18	122	Pyrazine, trimethyl	$C_7H_{10}N_2$	
17	13.33	99	2-Pyrrolidinone, 1-methyl	$C_5H_9NO$	
18	14.36	96	C2-alkyl imidazole or pyrazole	$C_5H_8N_2$	See 3
19	15.25	136	Pyrazine tetramethyl	$C_8H_{12}N_2$	
20	15.99	114	2-imidazolidinone-1,3-dimethyl	$C_5H_{10}N_2O$	
21	16.79	110	C3-alkyl imidazole or pyrazole	$C_6H_{10}N_2$	See 11
22	17.20-22	110, 124	C3/C4-alkyl imidazole or pyrazole	$C_6H_{10}N_2$ $C_7H_{12}N_2$	See 11

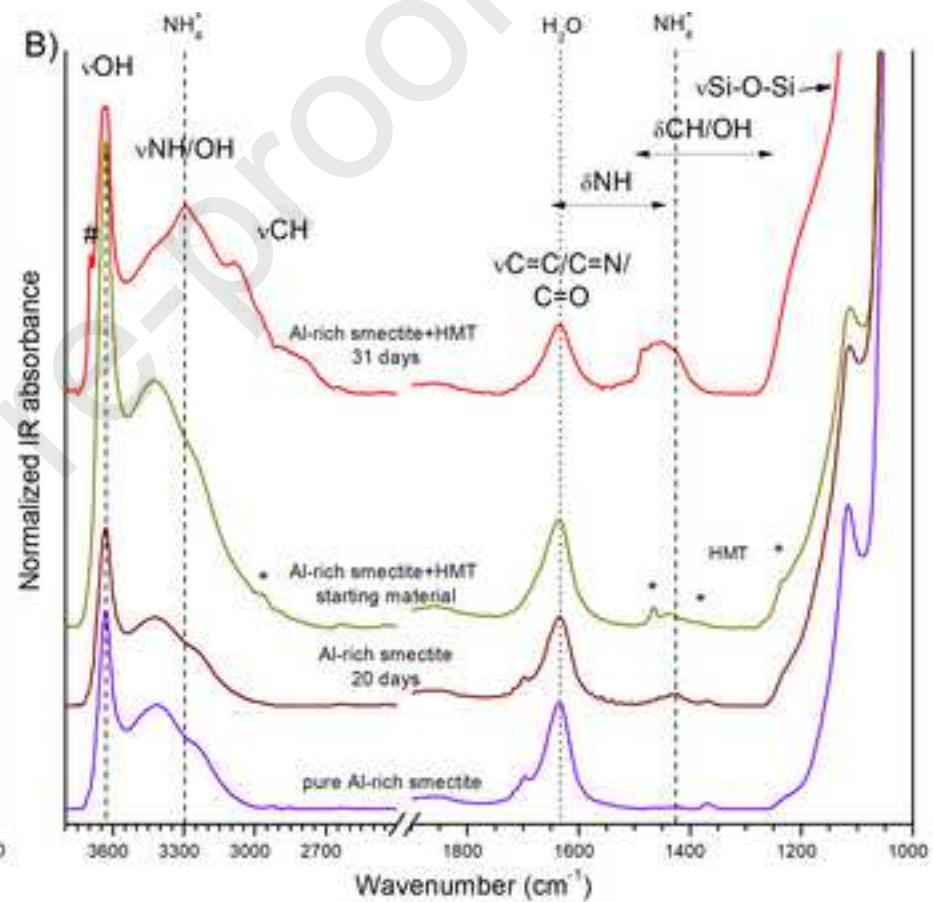
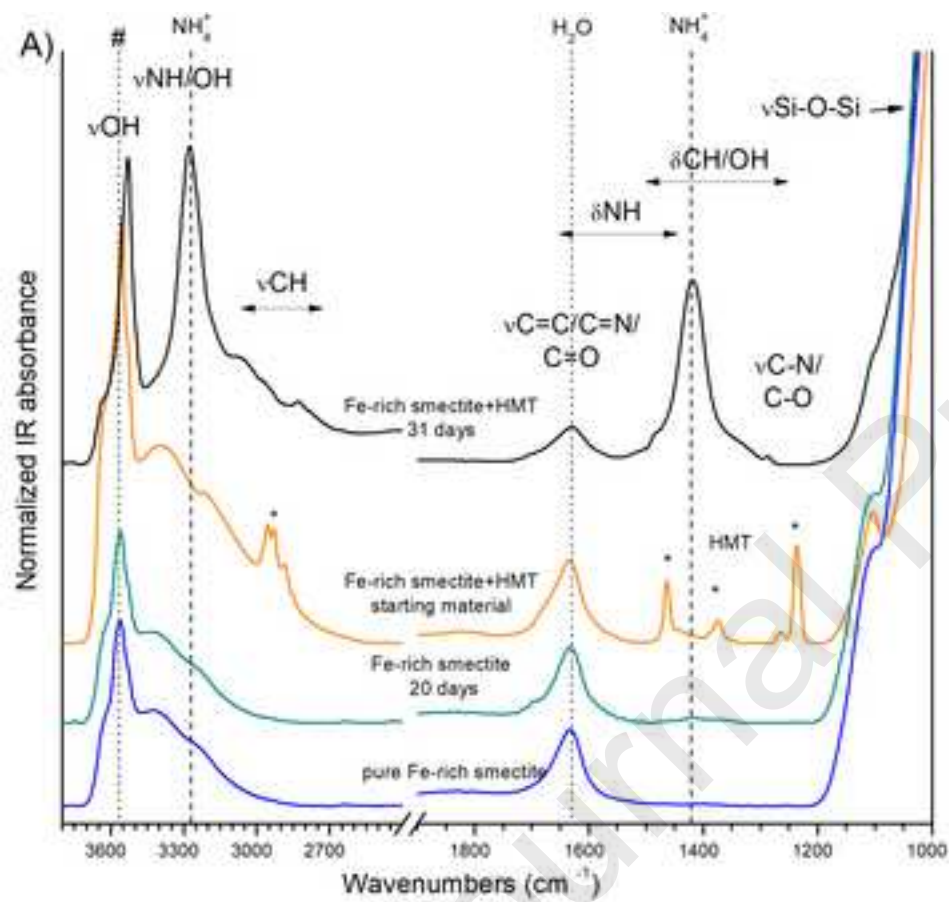
	$S_{\text{BET}}$ (m <sup>2</sup> /g)	$\tau$ (% HMT molecules)
Fe-rich smectite	42	<3
Al-rich smectite	77	<6

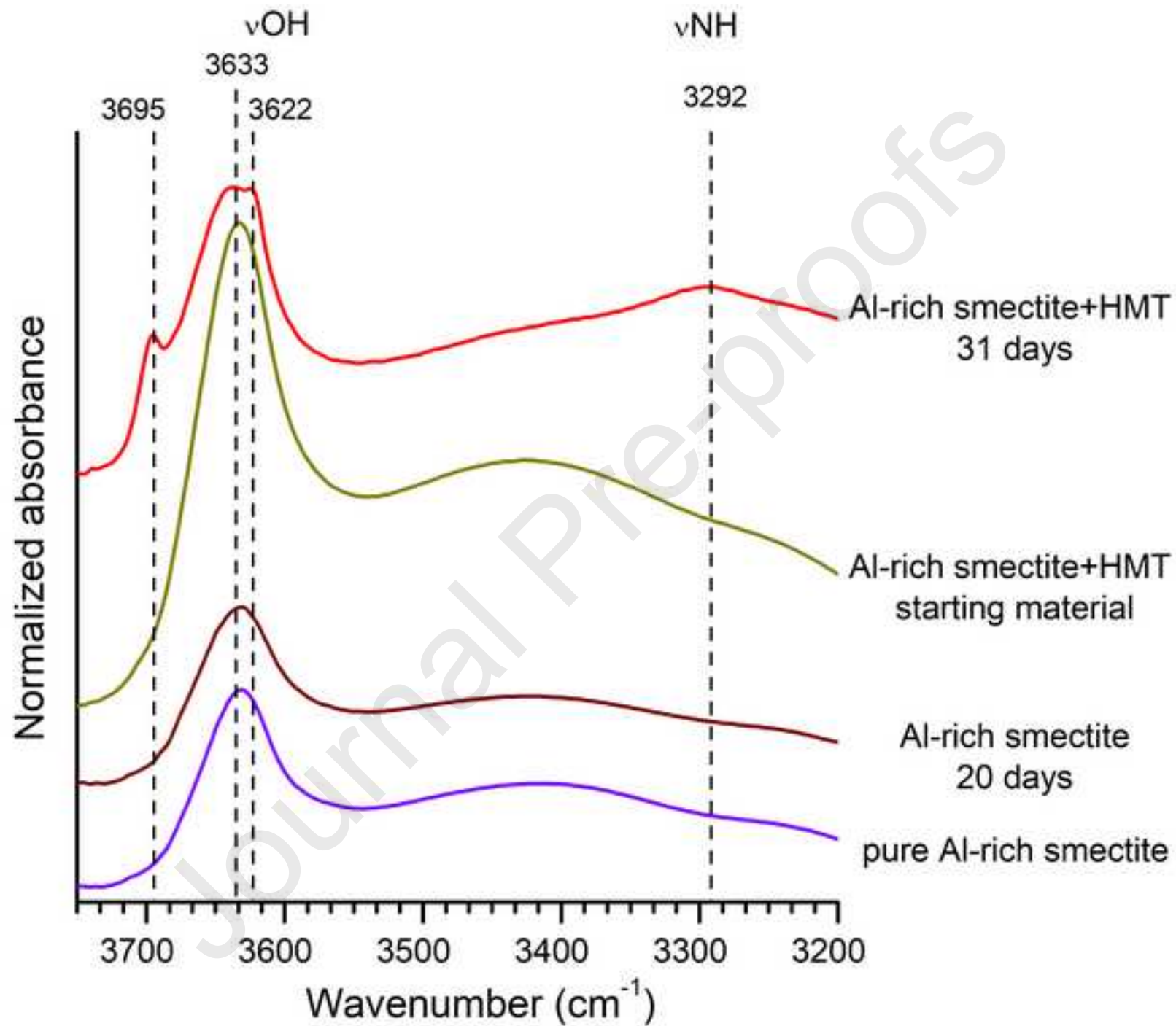
Sample after 31 days	C (wt.) ± 0.07	N (wt.) ±0.02	N/C	Total CNH (wt.)
From Fe-rich smectite	2.62	2.65	0.86	6.49
From Al-rich smectite	3.85	1.9	0.42	7.21

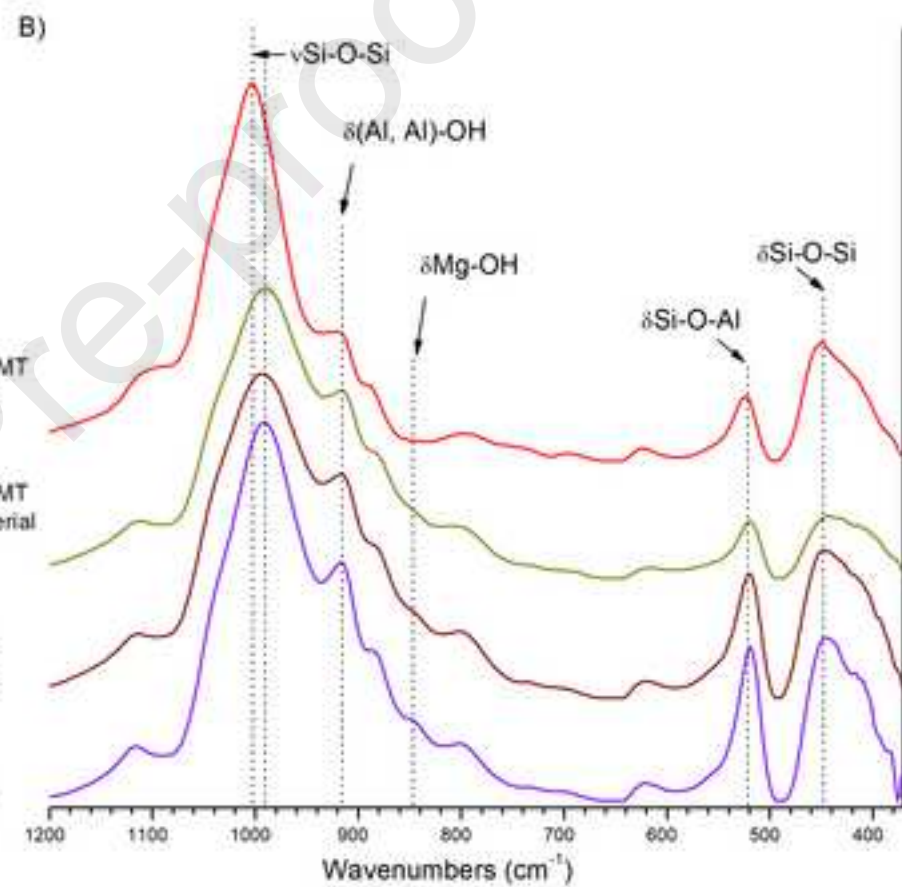
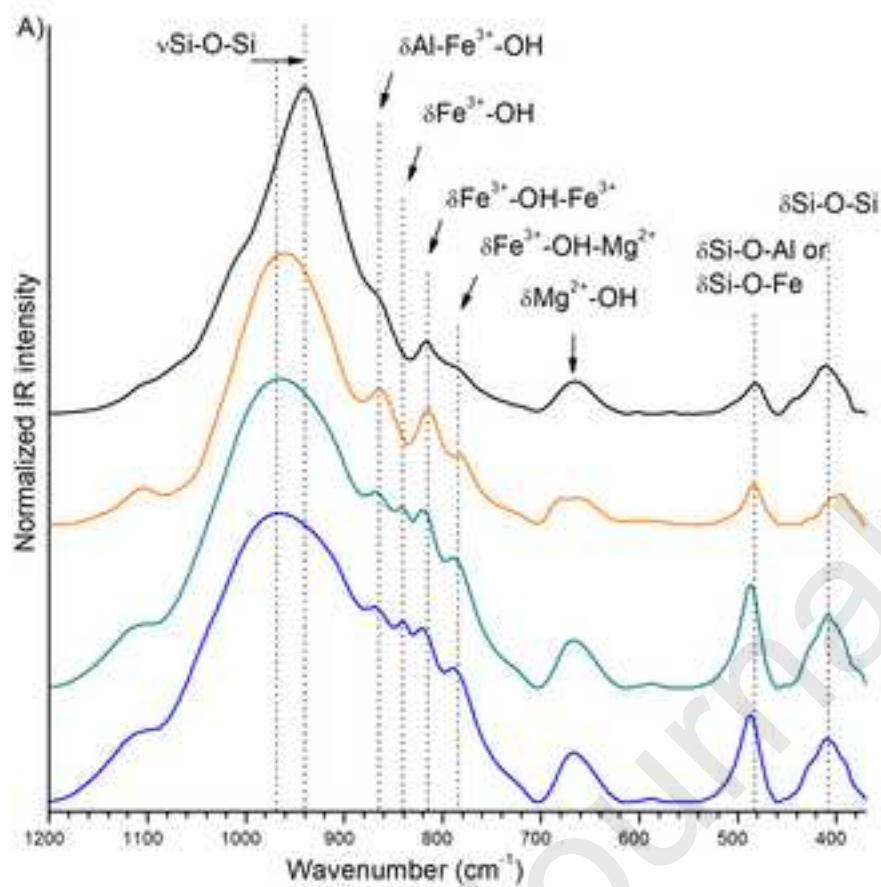


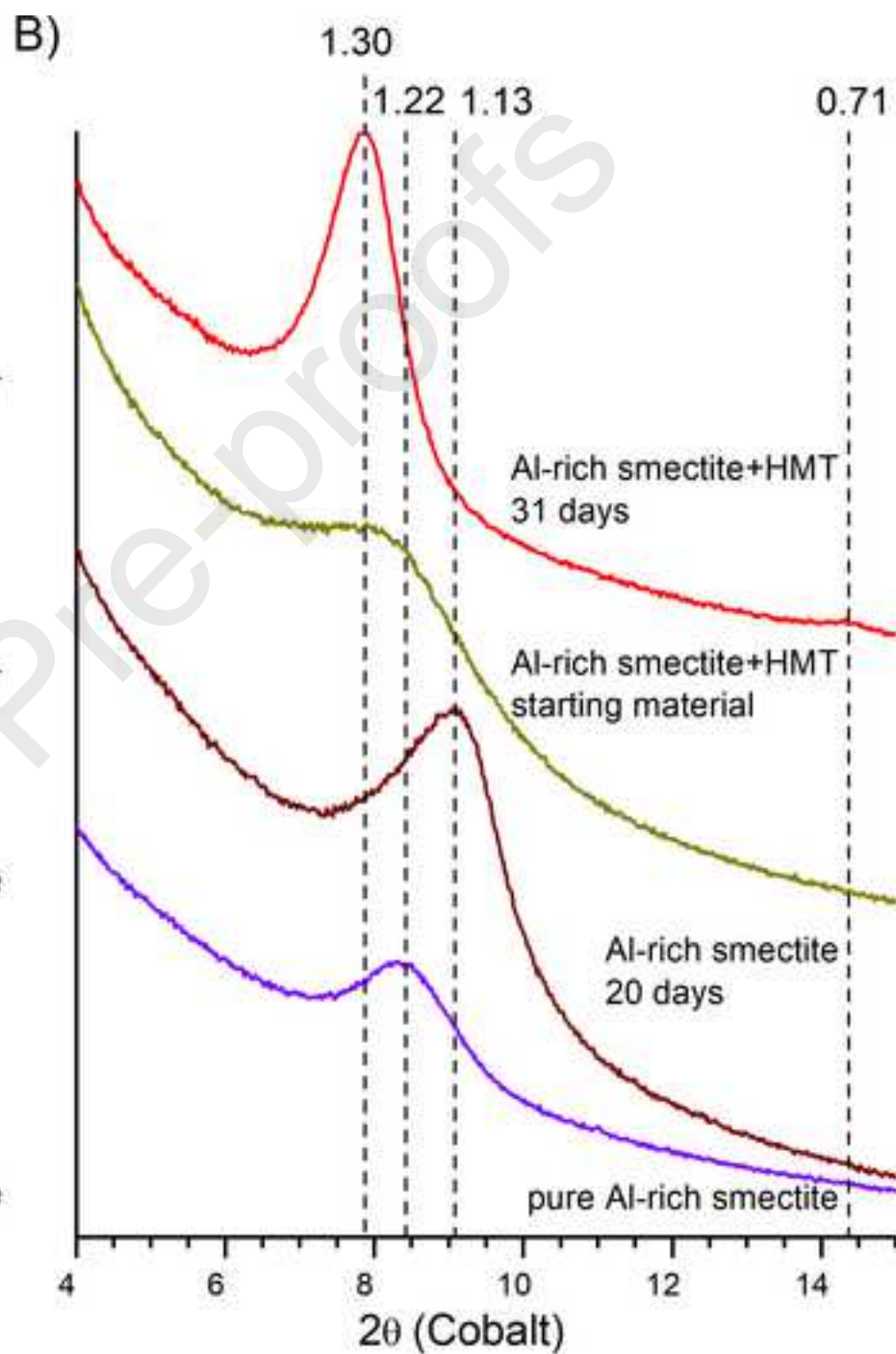
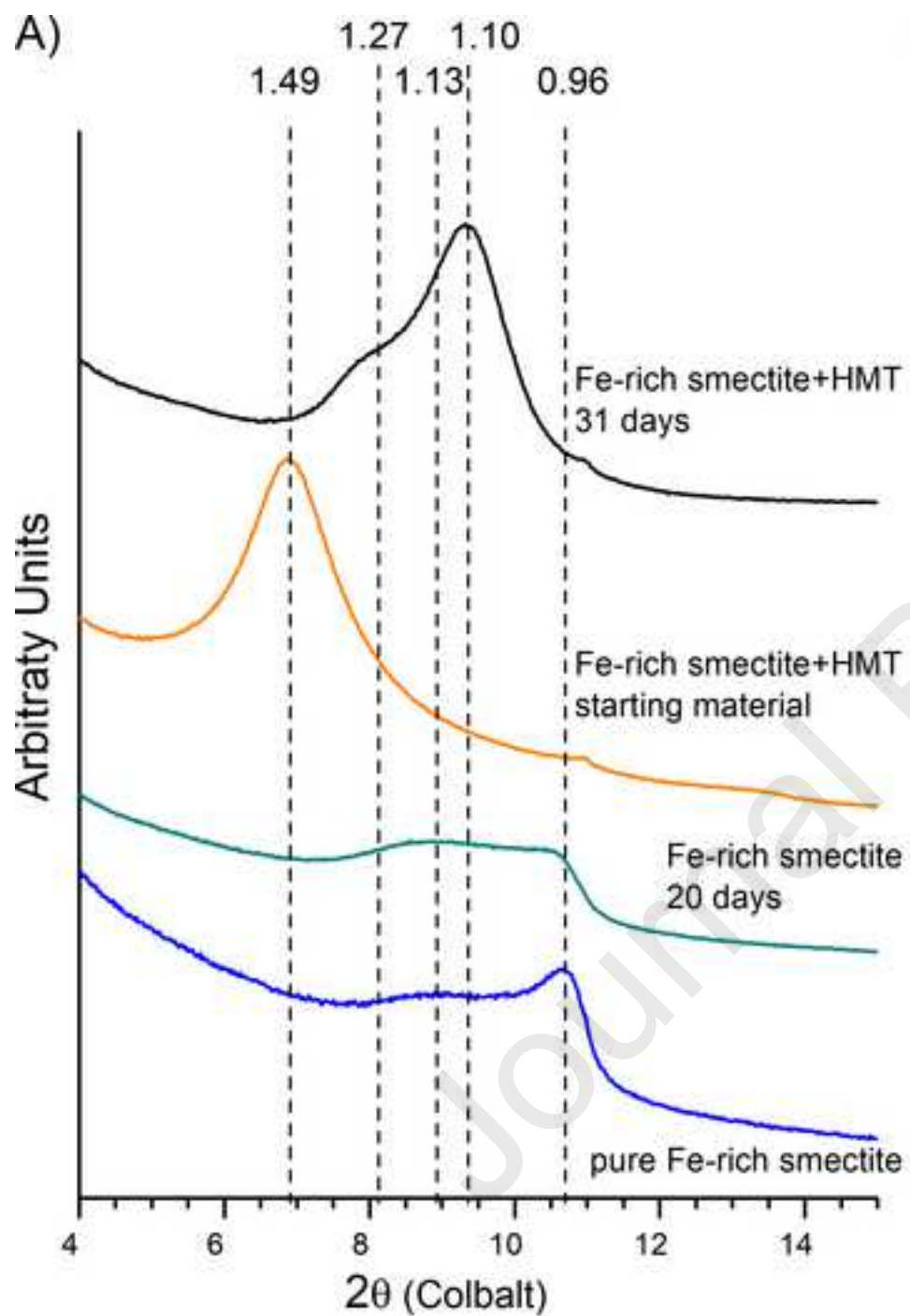












Phyllosilicate  
Organic matter

